



Cite this: *Nanoscale*, 2019, **11**, 10190

Received 20th March 2019,

Accepted 7th May 2019

DOI: 10.1039/c9nr02443c

rsc.li/nanoscale

Colloidal quasi-one-dimensional dual semiconductor core/shell nanorod couple heterostructures with blue fluorescence†

Dechao Chen,^a Aixiang Wang,^b Hongbo Li,^c Laura Abad Galán,^a Cong Su,^d Zongyou Yin,^e Massimiliano Massi,^a Alexandra Suvorova,^f Martin Saunders,^f Ju Li,^d Amit Sitt*^g and Guohua Jia^{b,*a}

Herein we report a nanorod couple heterostructure made of dual semiconductors, in which two parallelly aligned ZnSe nanorods are connected by the growth of ZnS on both end and side facets, producing hetero-ZnS (short arms)–ZnSe (long arms)/ZnS shell nanorod couples. As evidenced by electronic structure studies, both experimental and theoretical, such core/shell nanorod couple heterostructures can act as a platform to precisely tailor the quantum confinement of charge carriers between the constituting components within a single nano-object, generating blue fluorescence after the overgrowth of an alloyed ZnCdS layer on the heterostructures. We foresee the mechanistic insights gained and electronic structures revealed in this work would shed light on the rational design of more complex heterostructures with novel functionalities.

Introduction

Nano-heterostructures that integrate different components together to provide a system with unique dimensionality-

dependent integrative and synergic effects^{1–6} are of significant importance due to their diverse applications in solar energy harvesting,^{7,8} catalysis,^{9,10} electronics,^{11,12} biological imaging,^{13,14} and medical diagnostics and treatment.^{15,16} The recent advancements in the protocols of the colloidal synthesis enable the construction of multi-component structures with increasing chemical complexity that can be achieved in a predictable manner *via* a series of sequential synthetic procedures.^{1,2,12,17,18} In most cases, the preparation of heterostructures involves the sequential growth of one material onto another.^{1,2,18} However, heterostructures that are formed by the joining of two nano-components of the same composition together using a second material are less common in the literature.

As a benchmark heterostructure, CdSe-seeded CdS core/shell quantum rods with green to red fluorescence have received significant attention because they provide a platform for the stimulating studies of the elongated nanocrystals in a variety of applications in assemblies, photocatalysis, optoelectronic devices, and bio-labeling.^{19–23} However, due to the small bandgap of the core material of CdSe and the band offsets of the CdSe/CdS core/shell structure, it is difficult to tune the fluorescence of the CdSe/CdS core/shell quantum rod heterostructures into the blue spectral range. Manna and co-workers have developed a sequential cation exchange approach, in which the Cd²⁺ ion is replaced by Cu⁺ and then by Zn²⁺, to prepare blue-emitting ZnSe/ZnS core/shell quantum rods,²⁴ but this exchange is formed post synthesis and involves multiple steps. Hence, to date, the straightforward synthesis of semiconductor quantum rods with blue fluorescence remains highly challenging.

Herein, we report a wet-chemical method for fabricating hetero-ZnS (short arm)–ZnSe/ZnS core/shell (long arm) nanorod couples that are formed by bridging precisely two parallelly aligned ZnSe nanorods with ZnS at their edges. Mechanistic studies reveal that the formation of this heterostructure is attributed to the growth of ZnS between the end facets of each two parallelly aligned ZnSe nanorods, constitut-

^aCurtin Institute of Functional Molecules and Interfaces, School of Molecular and Life Sciences, Curtin University, GPO Box U1987, WA 6845, Australia.

E-mail: guohua.jia@curtin.edu.au

^bSchool of Chemistry and Chemical Engineering, Linyi University, Linyi 276005, China

^cSchool of Materials Science and Engineering, Beijing Institute of Technology, Haidian District, Beijing 100081, China

^dDepartment of Nuclear Science and Engineering and Department of Materials Science and Engineering, Massachusetts Institute of Technology, Cambridge, MA 02139, USA

^eResearch School of Chemistry, The Australian National University, Canberra, Australian Capital Territory 2601, Australia

^fCentre for Microscopy, Characterization and Analysis (CMCA) and School of Molecular Sciences, The University of Western Australia, Perth, WA 6009, Australia

^gRaymond and Beverly Sackler Faculty of Exact Sciences,

School of Chemistry Tel Aviv University, Tel Aviv 6997801, Israel.

E-mail: amitsitt@tauex.tau.ac.il

† Electronic supplementary information (ESI) available. See DOI: 10.1039/c9nr02443c

ing ZnS (short arms)–ZnSe/ZnS core/shell (long arms) nanorod couples. Effective mass approximation (EMA) simulations reveal that the electron occupies only ZnSe states, while the hole occupies a ZnS–ZnS state. Over-coating the nanorod couples with a layer of CdS produces ZnS–ZnSe/ZnCdS core/shell nanorod couples with blue fluorescence, in which the alloyed ZnCdS layer eliminates the surface traps and improves the quantum efficiency. The heterostructures were further converted into hetero-PbS (short arms)–PbSe (long arms)/PbS nanorod couples through a cation exchange reaction.

Results and discussion

Controlled synthesis and growth mechanism of hetero-ZnS (short arm)–ZnSe/ZnS core/shell (long arm) nanorod couples

The hierarchical self-assembly processes in the growth of nanorod couples allow the separation of the intermediate products from the reaction system and the manipulation of the particle growth in a controlled manner.^{25,26} We took advantage of this by incorporating both Zn and S precursors together with the purified ZnSe nanorods into the reaction system to synthesize hetero-ZnS (short arm)–ZnSe/ZnS core/shell (long arm) nanorod couples (Fig. 1a). Surprisingly, after the reaction evolved for 30 seconds, Zn (zinc nitride) and S precursors (1-dodecanthiol) integrated two ZnSe nanorods into a single hetero-nanorod couple (Fig. 1b) by the growth of ZnS on both end facets of two parallelly aligned ZnSe nanorods (Fig. 1c). Further growth of ZnS islands on the side facet of the long arms was obtained as the reaction continued (Fig. 1d). Analogous to the previously reported single-component ZnSe nanorod couples,²⁶ the driving forces responsible for the initial pairing of ZnSe nanorods with ZnS are dipole–dipole and crystal–crystal interactions. The pairing of ZnSe rods *via* bridging both end facets by ZnS is formed *via* a self-limited assembly mechanism, because once the end facets of ZnSe are blocked by the growth of ZnS, the hetero-ZnSe–ZnS nanorod couple cannot interact with another ZnSe nanorod.²⁶ Upon the growth of the ZnS shell, the absorption onset exhibits a slight red shift of 7 nm as a result of the leakage of the excitonic wave function into the ZnS layer.^{27,28} A prolonged reaction time of 30 minutes (Fig. 1d) produced branched hetero-ZnS–ZnSe/ZnS nanorod couples with ZnS decorating the surface of the nanorod couple heterostructures. The corresponding absorption onset is slightly smeared, but clearly, a further red shift is observed. The island growth of ZnS at prolonged time may be a result of the lattice strain existing between the interfaces of the ZnSe and ZnS,²⁹ which may also result in the red shift of absorption as previously observed in ZnSe/ZnS core/shell nanoparticles.³⁰ Particle size analysis (Fig. S1†) shows that the lengths of the original (Fig. 1b), intermediate (Fig. 1c) and final nanorods (Fig. 1d) are almost constant (72.0 nm to 78.7 nm), but their widths change from 2.5 nm to 5.6 nm, and then to 7.5 nm. The increase of width correlates to both the growth of ZnS on both end and side facets of two parallelly aligned ZnSe nanorods. A distinct spacing between two rod

components (Fig. 1c and d) is seen, which can be attributed to the steric hindrance of the oleylamine ligands passivating on the surface of each rod component. Energy dispersive X-ray (EDX) spectroscopy analysis shows that the atomic ratio of Se:S decreases as a function of the reaction time (Fig. 1f), which is consistent with the growth of ZnS on the ZnSe nanorod components. The powder X-ray diffraction (XRD) patterns of hetero-ZnS–ZnSe/ZnS core/shell nanorod couples present a shift to higher angles with respect to those of pure ZnSe, which further confirms the growth of the ZnS (Fig. 1g). Using bis(trimethylsilyl)sulfide as the sulfur source instead of 1-dodecanethiol while keeping other synthetic conditions constant also produced hetero-ZnS–ZnSe/ZnS core/shell nanorod couples (Fig. S2†) with an even smaller spacing between the two ZnSe rods. The high activity of bis(trimethylsilyl)sulfide leads to the fast growth of ZnS and its high etching capability at elevated temperatures may result in such a small spacing between each rod components of the hetero-nanorod couples.³¹ This demonstrated the generality of this synthetic approach for compositing hetero-nanorod couples. The above control experiment also demonstrated that two elongated nanorods can be integrated into a single nano-object in a pre-defined way through material engineering and optimization of synthetic protocols.

We used transmission electron microscopy (TEM) imaging in combination with fast Fourier transform (FFT) analysis to reveal how hetero-ZnS–ZnSe/ZnS core/shell nanorod couples form from two parallelly aligned ZnSe nanorods in the presence of Zn and S precursors. Fig. S2a and S3† show the branched hetero-ZnS–ZnSe/ZnS core/shell nanorod couples with different dimensions. Close inspection of the connecting areas of the heterostructures (labelled by the dashed red rectangle in Fig. 2a, S4a and S4f†) shows that a single hetero-structure is formed through ZnS growth on both end facets of two parallelly aligned ZnSe nanorods. The (111) plane of zincblende ZnS grows on the (0002) plane of wurtzite ZnSe nanorods, creating the connecting areas (Fig. 2b, S4b and S4g†), as confirmed by the presence of two sets of diffraction patterns (Fig. 2d, S4d and S4i†) of both zincblende ZnS (Fig. 2e, S4e and S4j†) and wurtzite ZnSe (Fig. 2c, S4c and S4h†) in close proximity of the boundary. We attribute the growth of (111) zincblende ZnS on the (0002) plane of the ZnSe wurtzite to the moderate lattice mismatch between these two planes, which is about 3.9% (Table S1†).^{32–34} Based on the above diffraction analysis, we propose the atomistic crystal structure shown in Fig. 2f to explain how the short arms of zincblende ZnS join the end facets of two parallelly aligned ZnSe nanorods.

The orientation of the crystal lattices of branched structures is similar to that of the ZnSe rod couples, as is confirmed by HRTEM characterization (Fig. 2g and S5†) and the FFT analyses (insets of Fig. S5†). An evident spacing between the rods is observed in individual hetero-ZnS–ZnSe nanorod couples (Fig. S6–S8†). The boundaries of the nanorod couples, and in particular the gap between them, became more evident after coating of the hetero-ZnS–ZnSe/ZnS core/shell nanorod couples with a shell layer of CdS (Fig. 2h) (see the

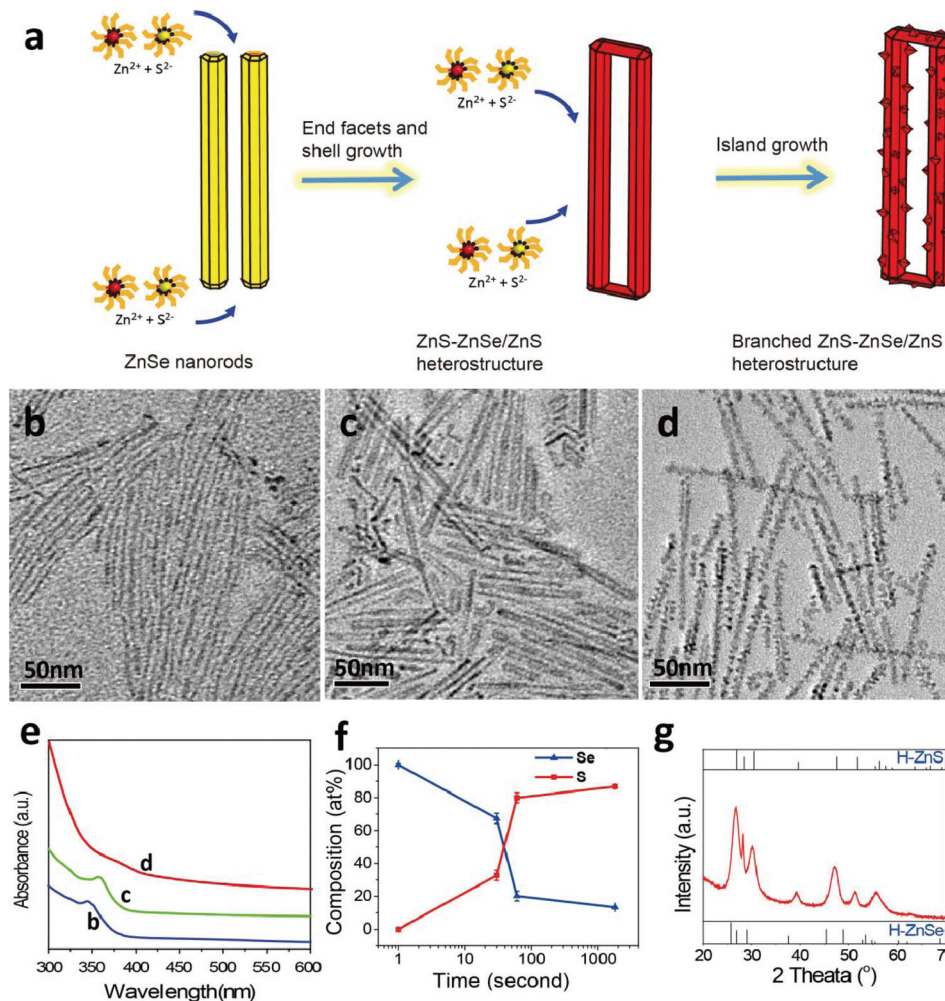


Fig. 1 (a) A schematic illustration showing a controlled synthesis of ZnS (short arms)–ZnSe/ZnS core/shell (long arms) heterostructures. (b–d) TEM images of (b) the original thin ZnSe nanorods, (c) the hetero-ZnS–ZnSe/ZnS core/shell nanorod couples obtained after 30 seconds at 280 °C, and (d) the branched hetero-ZnS–ZnSe/ZnS core/shell nanorod couples obtained after 30 minutes at 280 °C. (e) Absorption spectra corresponding to (b–d). (f) Chemical composition of Se (%) and S (%) of branched hetero-ZnS–ZnSe/ZnS core/shell nanorod couples as a function of the reaction time (1 second, 30 seconds, 1 minute and 30 minutes, respectively). (g) XRD patterns of branched hetero-ZnS–ZnSe/ZnS core/shell nanorod couples.

Experimental section in the ESI† for details). This is mainly a result of the surface reconstruction of the branched ZnS structures on the surface of the hetero-nanorod couples, which occurs at the high growth temperature that is required for the CdS shell growth.

High-angle annular dark field-scanning transmission electron microscopy (HAADF-STEM) confirms the formation of the branched structures on the surface of hetero-ZnS–ZnSe/ZnS core/shell nanorod couples (Fig. 3a). Some particles that resemble single rods can also be identified in the micrograph, but they exhibit a higher contrast, which indicates that these are rod couples, which are positioned in a perpendicular alignment on top of amorphous carbon film (Fig. 3a). HAADF-EDX element mapping confirms the presence of Zn, Se and S elements in the hetero-nanorod couples (Fig. 3b and S9†) and Zn^{2+} ions are evenly distributed throughout the elongated

nanoparticles (Fig. 3b). Close inspection on the element maps of Se^{2-} and S^{2-} ions indicates that Se^{2-} ions are predominately distributed on the inner side of the obtained nanorod couples whereas S^{2-} ions are initially located on the outer side of the nanoparticles. This confirms the formation of ZnS–ZnSe/ZnS core/shell nanorod couples accompanied with the extensive growth of ZnS branched structures on the ZnSe rod components. Apparently, the mapping of the Se element is weak, which is consistent with the low molar ratio of Se (~13%) in the branched hetero-ZnS–ZnSe/ZnS core/shell nanorod couples (Fig. 1f). The Z-contrast STEM image (Fig. 3c) shows that the spacing between two rod components is not continuous and may be interrupted by fusing the adjacent facets of two rods. This image also confirms that ZnS-branched structures have grown on both exterior sides and the interior sides of the rod components of nanorod couples.

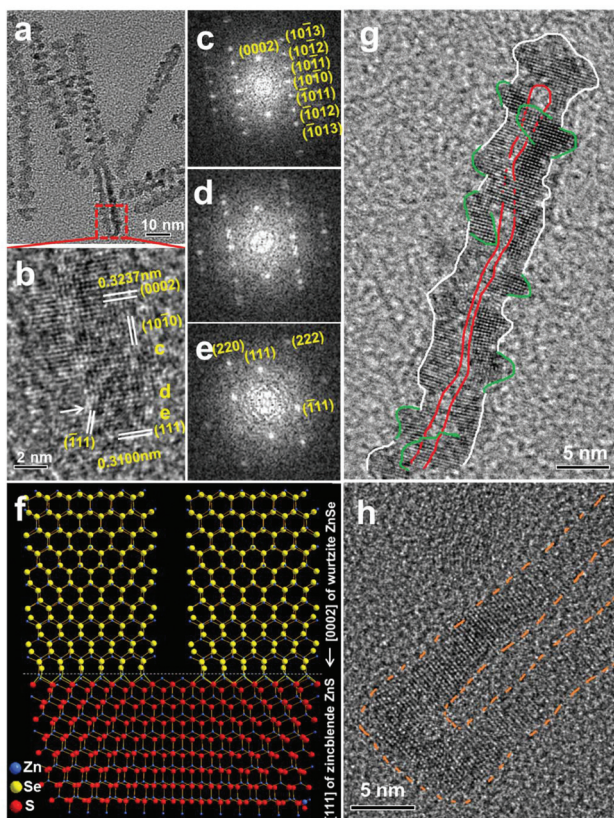


Fig. 2 (a) TEM image. (b) HRTEM image of the short arm marked by a dashed rectangle in (a). The boundary between wurtzite hexagonal (H-) ZnSe and zincblende cubic (C-) ZnS is labelled by an arrow. (c–e) FFT of selected areas in (b) revealing the crystallographic relations. The diffraction patterns in (c) and (e) match H-ZnSe and C-ZnS, respectively. (f) Schematic atomic crystal structure corresponding to the region depicted in (b). (g) HRTEM image of an individual branched nanorod couple. White lines outline the boundary of the branched nanorod couple, green lines outline the ZnS branches, and red lines outline the gap between two rods. (h) HRTEM image of the branched hetero-ZnS-ZnSe/ZnS/CdS core/shell/shell nanorod couples revealing a clear gap (marked by dashed orange lines) between two rods.

One of the intriguing questions regarding the presented system is why the growth of ZnS on the surface of hetero-ZnS-ZnSe nanorod couples leads to branched structures. Obviously, this is not due to the compatibility between these two materials since the lattice mismatch between ZnS (wurtzite) and ZnSe (wurtzite) is not very large (4.5%) (Table S1†). In a control experiment, ZnSe nanorods were dissolved into the same reaction solvent in the presence of the same sulfur precursor, *i.e.* 1-dodecanethiol, at a reaction temperature of 280 °C. Under these conditions, the ZnSe nanorods were partially etched, leading to rods with rough surface facets (Fig. S10†). This process highly resembles the etching of CdS nanorods in the presence of zinc oleate.³⁵ Thus we believe that in the case of the ZnS-ZnSe/ZnS nanorod couples, the surface of the ZnSe rods is etched, and at the same time, ZnS grows epitaxially on the rough surface facets of the nanorod couples, leading to the formation of branched structures.

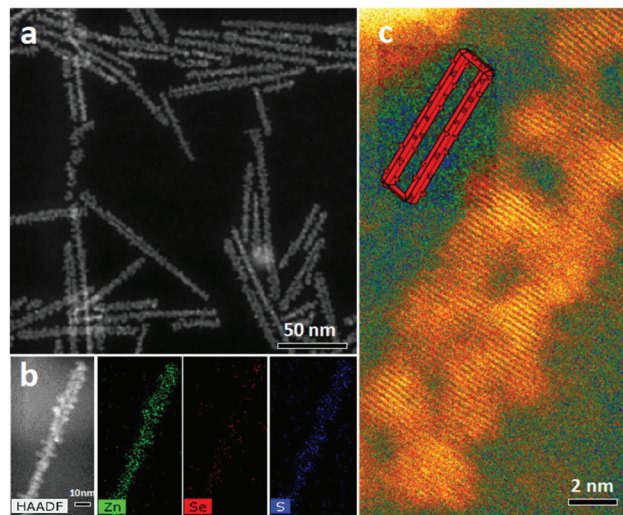


Fig. 3 (a) HAADF-STEM image of hetero-ZnS-ZnSe/ZnS core/shell nanorod couples showing a spacing between each of the two rods. (b) HAADF-STEM image and elemental maps of an individual hetero-ZnS-ZnSe/ZnS core/shell nanorod couple. (c) A high-resolution Z-contrast STEM image of an individual hetero-ZnS-ZnSe/ZnS core/shell nanorod couple.

It is worth noting that the structure of the zinc blende ZnS short arms connecting the end facets of two parallel ZnSe nanorods is different from that of the wurtzite ZnS shell grown on the side facets of the ZnSe nanorods. This can be explained by the relatively small difference in the total energy between the zinc blende and wurtzite phases of ZnS (3.1 meV per atom)³⁶ and the different types of growth of ZnS with respect to the pre-existing ZnSe. In the former case, the growth of the zinc blende-structured ZnS on the wurtzite-structured ZnSe nanorods only occurred on a small region, *i.e.* the most reactive end facets of ZnSe nanorods. This is unlikely to lead to a substantial lattice strain at the interfaces between the short ZnS arms and the end facets of ZnSe nanorods. In addition to the effect of lattice mismatch, the kinetic effect of reaction precursors may also affect the phase of ZnS because the crystallization of zinc blende-structured ZnS is preferred at high supersaturation of zinc and sulfur precursors.^{37–39} However, in the latter case, wurtzite-structured ZnS growth on the elongated side facets of wurtzite-structured ZnSe is preferred because this can significantly reduce the lattice strain and increase the stability of the core/shell structure.

Electronic structure of hetero-ZnS (short arm)-ZnSe/ZnS core/shell (long arm) nanorod couples

The transition from homo-ZnSe nanorod couples to hetero-ZnS-ZnSe/ZnS nanorod couples leads to a significant change in the envelope wave functions of the charge carriers and in the energy level structure. A numerical finite-well EMA approach was employed to study the electronic structure of the hetero-ZnS-ZnSe/ZnS nanorod couples (Fig. 4, Table S2, also see the ESI† for details). In homo-ZnSe nanorod couples, the

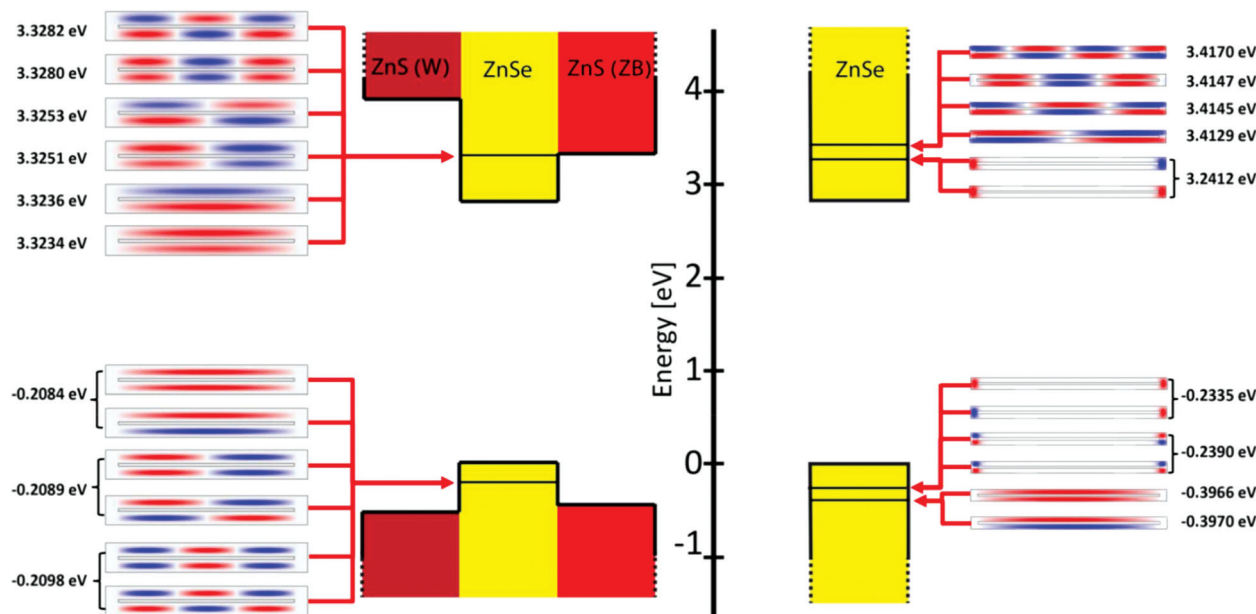


Fig. 4 Electronic structures of hetero-ZnS–ZnSe nanorod couples (left panel) compared with homo-ZnSe nanorod couples (right panel). Magnifications of the near band-edge energy levels and envelope wavefunctions of electron and hole states are depicted in top and bottom panels, respectively. The wavefunctions are portrayed at the cross-section along the xz plane ($y = 0$). White is 0, and red and blue are the + and – phases, respectively. Electron and hole states are presented in different energy scales for clarity.

wavefunctions of the lowest electron/hole states reside in the corners of the nanorod couples (right panel of Fig. 4), while in the hetero-ZnS–ZnSe nanorod couples they reside in the long vertices (left panel of Fig. 4). From the shape and position of the lowest six electronic and hole states, they can be clearly characterized as ZnSe rod states. However, because the electron states energies reside above the conduction band offset of ZnSe–ZnS (ZB), the penetration of the electron states into the short edges is slightly more pronounced. Within the first 6 states, in the ZnSe there is a relatively large energy difference between the “corner” states and the long edge states, which is a result of the lower confinement of the charge carriers in the corners of the structure. On the contrary, in the hetero-ZnS–ZnSe system, all the states are almost degenerate because they are “rod” states. It is worth noting that the formation of the ZnS shell on the hetero-ZnS–ZnSe nanorod couples further strengthens the confinement of holes into the ZnSe nanorod components of the hetero-nanorod couples, while the electrons leak much more into the ZnS (W) shell, mainly because of the lower effective mass of the electron.

Optical properties of hetero-ZnS–ZnSe/ZnCdS core/shell nanorod couples

The above EMA simulations show that the electronic structures of the hetero-ZnS–ZnSe core/shell nanorod couples should present a distinct change in the luminescence characteristics compared to those of the homo-ZnSe nanorod couples (Fig. 4). In order to eliminate surface traps and to increase the quantum efficiency, a CdS layer was grown on the nanorod couples, generating hetero-ZnS–ZnSe/ZnCdS core/shell

nanorod couples. TEM measurements confirmed that the obtained homo-ZnSe/CdS (Fig. 5a1) and hetero-ZnS–ZnSe/ZnCdS core/shell nanorod couples (Fig. 5a2) retain the distinct features of the original particles (Fig. S11a and S12a†). Statistical analysis of the nanoparticles before and after the CdS shell growth shows that 1–4 monolayers of CdS were grown (Fig. S11b and S12b†). As depicted in Fig. 5b1, ZnSe/CdS nanorod couples constitute core/shell structures with a type II configuration, and therefore, a significant red shift of the band gap with respect to the original ZnSe is expected. The excitation spectra are broader (green curves in Fig. 5c1) and resemble the respective absorption spectrum. The corresponding Stokes shift is large (62 nm) with respect to that of CdS rods (~ 4 –10 nm, Fig. S13†), consistent with previous results reported in the literature.^{40–42}

In contrast, the band structures of hetero-ZnS–ZnSe/ZnS core/shell nanorod couples have a quasi-type I configuration because the electron wave functions slightly penetrate the ZnS while the holes are predominantly confined inside the ZnSe nanorod components (Fig. 5b2), as predicted by the EMA simulations (Fig. 4). The formation of an alloyed layer of ZnCdS on hetero-ZnS–ZnSe nanorod couples pushes down the band edge of the conduction band slightly (Fig. 5b2). As a result, a small red shift in both absorption and emission spectra in comparison with those of homo-ZnSe/CdS core/shell nanorod couples is expected. As for the hetero-ZnS–ZnSe/ZnCdS core/shell nanorod couples, interestingly, the luminescence excitation spectrum (green curve in Fig. 5c2) matches the absorption spectrum of the original hetero-ZnS–ZnSe/ZnS nanorod couples. The emission of the hetero-ZnS–ZnSe/ZnCdS

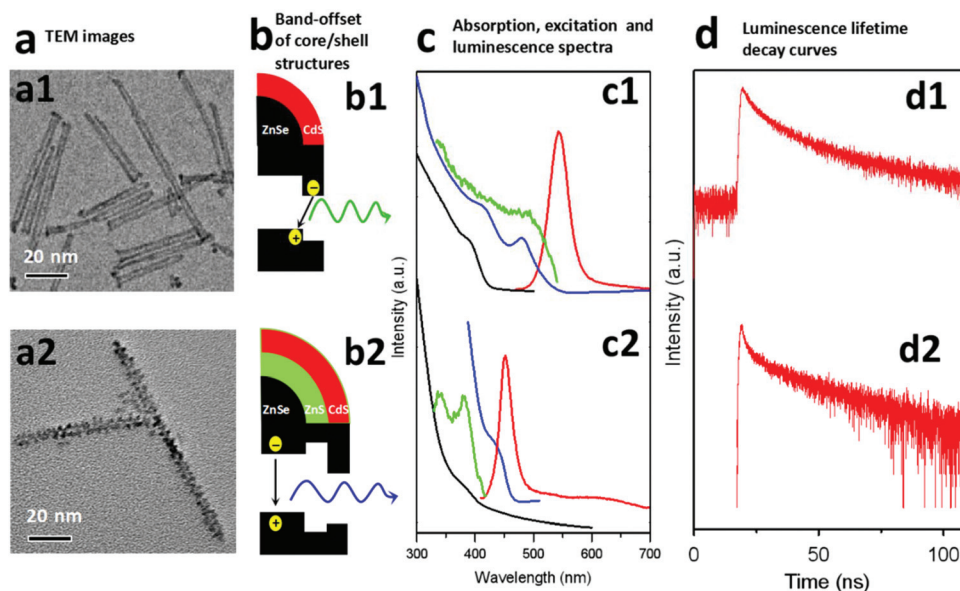


Fig. 5 (a) TEM images. (b) Band offset of core/shell structures. (c) Optical spectra. (d) Fluorescence lifetime decay curves at room temperature. (a1–d1) Homo-ZnSe nanorod couples. (a2–d2) Branched hetero-ZnS (short arm)–ZnSe (long arm)/ZnCdS core/shell/shell nanorod couples.

core/shell nanorod couples falls in the blue range with a peak at 451 nm and the Stokes shift is 10 nm. This shift is much smaller than that of homo-ZnSe/CdS core/shell nanorod couples with a type II configuration (Fig. 5c1) and is consistent with the aforementioned band offset analysis. It is worth noting that the strain existing at the interfaces between ZnS and CdS may also lead to a red shift, as observed in core/shell nanoparticles.³²

We also compared the luminescence spectra of the nanorod couples before and after CdS shell growth (Fig. S14a†). In this case, luminescence of the original nanorod couples was obtained by performing the surface ligand exchange from oleylamine to trioctylphosphine (TOP). After CdS shell growth, the shifts of the luminescence peak of the homo-ZnS–ZnSe/CdS nanorod couples (Fig. S14a†) were 120 nm, whereas the shift for hetero-ZnS–ZnSe/ZnCdS core/shell nanorod couples (Fig. S14b†) was 44 nm. The luminescence spectra for all core/shell nanorod couples measured at 77 K exhibit a blue shift compared with those measured at room temperature (Fig. S15 and S16†), which is consistent with the reduction of thermal smearing.

The quantum efficiency of the hetero-ZnS–ZnSe/ZnCdS core/shell nanorod couples is ~2%, which is much lower than those of homo-ZnSe/CdS nanorod couples (15%) (Table S3†). This is most likely because forming a perfect CdS shell over the branched ZnS structures in hetero-ZnS–ZnSe/ZnS nanorod couples is hard to achieve, and defects, which act as trap states for the electrons and holes, are not diminished. Fluorescence lifetimes of all core/shell nanorod couples at both room temperature and 77 K were measured and compared in Fig. 5d and S17.† The time-resolved fluorescent decay curves were fitted by a bi-exponential model, $I(t) = A_1[-t/\tau_1] + A_2\exp[-t/\tau_2]$. For hetero-ZnS–ZnSe/ZnCdS nanorod couples, $\tau_1 = 6.0$ ns and $\tau_2 =$

45.3 ns whereas $\tau_1 = 10.3$ ns and $\tau_2 = 50.5$ ns for homo-ZnSe/CdS nanorod couples at room temperature (Table S3†). The fluorescent lifetimes are much shorter at 77 K (Fig. S17†) compared with those at room temperature as the possibility for non-radiative transition is significantly reduced at low temperature. Although the hetero-ZnS–ZnSe/ZnCdS core/shell nanorod couples show a much lower quantum efficiency than homo-ZnSe/CdS nanorod couples, the luminescence and luminescence excitation spectra of the former provide sufficient information to reveal the distinct change in the luminescence characteristics between hetero- and homo-nanorod couples.

We further expanded this distinct hetero-nanorod couples into other compositions by a cation exchange reaction (Fig. S18a†).^{43–45} We specifically targeted lead ions (Pb^{2+}) since we are most likely to observe the electronic coupling effect between two closely spaced PbSe rods within a hetero-PbS (short arms)–PbSe (long arms) nanorod couple. This is because the wavefunctions of electrons and holes in PbSe are more delocalized considering its larger exciton Bohr radii (46 nm)⁴⁶ in comparison with the small Bohr exciton radius of ZnSe (4.5 nm).⁴⁷ TEM (Fig. S18b and S18c†) and HAADF-STEM (Fig. S18d and S18e†) imaging confirmed that the produced nanoparticles maintained the original features of the branched hetero-nanorod couples. STEM-EDX maps confirmed the alternation of the composition of the hetero-nanorod couples (Fig. S19†). FFT analysis of the selected area in the HRTEM image (Fig. S18c†) and XRD patterns corroborate the rock-salt structure of the crystal lattice of the obtained nanoparticles (Fig. S18g†). The absorption features at longer wavelength (2 in Fig. S18f†) are consistent with the small bandgap of PbS–PbSe. The hetero-PbSe–PbS/PbS nanorod couples do not show any detectable PL as the emission intensity in the near-infrared

spectral range may be too weak to be detected. The structural analysis and EDX measurement confirm the successful expansion of hetero-PbS–PbSe nanorod couples *via* a cation exchange reaction, which provides an ideal platform to study the electronic coupling effects between closely spaced nanorods. Further experiments in this area are in progress.

Conclusions

In conclusion, we have demonstrated a facile wet-chemical approach for the synthesis of hetero-ZnS–ZnSe nanorod couples with ZnS precisely grown on the end facets of two parallel aligned ZnSe nanorods. Due to the small contact area between ZnSe and ZnS at the apexes of ZnSe nanorods, the growth of zincblende ZnS on ZnSe nanorods may still be epitaxial. The hetero-ZnS–ZnSe/ZnCdS core/shell nanorod couples show a blue emission due to the distinct quantum confinement regime within these unique heterostructures in comparison with the green emission from homo-core/shell nanorod couples. Further expanding the hetero-nanorod couples produced hetero-PbS–PbSe/PbS nanorod couples. The synthetic strategy developed here may provide new insight into the rational design and synthesis of new heterostructures with increasing complexity, and the heterostructures obtained here may facilitate the incorporation of such materials into optoelectronic and catalytic applications.

Conflicts of interest

There are no conflicts to declare.

Acknowledgements

G. J. conceived the project, designed the experiments and supervised the research. D. C. conducted synthesis, materials characterization and analysis. A. S. performed the EMA simulations. C. S. measured the Z-contrast STEM of the samples and Z. Y. and J. L. analysed the data. H. L., A. W., A. S. and D. C. prepared the figures and ESI[†] sections. L. A. G. and M. M. measured the optical spectroscopy of the materials. A. S. and M. S. assisted with HRTEM measurements and structural analysis. G. J. and A. S. wrote the manuscript. All authors discussed the data, mechanisms, and commented on the manuscript. This work was supported by the Australian Research Council (ARC) Discovery Early Career Researcher Award (DECRA) (Project ID: DE160100589), and the National Natural Science Foundation of China (Grant No. 21701015 and 21811530054). The authors acknowledge the facilities, and the scientific and technical assistance of the Australian Microscopy & Microanalysis Research Facility at the Centre for Microscopy, Characterisation & Analysis, The University of Western Australia, a facility funded by the University, State and Commonwealth Governments.

Notes and references

- 1 R. Costi, A. E. Saunders and U. Banin, *Angew. Chem., Int. Ed.*, 2010, **49**, 4878–4897.
- 2 G. Jia, Y. Pang, J. Ning, U. Banin and B. Ji, *Adv. Mater.*, 2019, **31**, 1900781.
- 3 K. Wu, J. Chen, J. R. McBride and T. Lian, *Science*, 2015, **349**, 632–635.
- 4 P. Li, Z. Wei, T. Wu, Q. Peng and Y. Li, *J. Am. Chem. Soc.*, 2011, **133**, 5660–5663.
- 5 R. D. Robinson, B. Sadtler, D. O. Demchenko, C. K. Erdonmez, L.-W. Wang and A. P. Alivisatos, *Science*, 2007, **317**, 355–358.
- 6 U. Banin, Y. Ben-Shahar and K. Vinokurov, *Chem. Mater.*, 2014, **26**, 97–110.
- 7 A. Vaneski, A. S. Susha, J. Rodríguez-Fernández, M. Berr, F. Jäckel, J. Feldmann and A. L. Rogach, *Adv. Funct. Mater.*, 2011, **21**, 1547–1556.
- 8 Y. Shemesh, J. E. Macdonald, G. Menagen and U. Banin, *Angew. Chem., Int. Ed.*, 2011, **123**, 1217–1221.
- 9 T. Simon, N. Bouchonville, M. J. Berr, A. Vaneski, A. Adrovic, D. Volbers, R. Wyrwich, M. Döblinger, A. S. Susha, A. L. Rogach, F. Jäckel, J. K. Stolarczyk and J. Feldmann, *Nat. Mater.*, 2014, **13**, 1013–1018.
- 10 S. M. Kim, S. J. Lee, S. H. Kim, S. Kwon, K. J. Yee, H. Song, G. A. Somorjai and J. Y. Park, *Nano Lett.*, 2013, **13**, 1352–1358.
- 11 N. Oh, B. H. Kim, S.-Y. Cho, S. Nam, S. P. Rogers, Y. Jiang, J. C. Flanagan, Y. Zhai, J.-H. Kim, J. Lee, Y. Yu, Y. K. Cho, G. Hur, J. Zhang, P. Trefonas, J. A. Rogers and M. Shim, *Science*, 2017, **355**, 616–619.
- 12 R. Lavieville, Y. Zhang, A. Casu, A. Genovese, L. Manna, E. Di Fabrizio and R. Krahne, *ACS Nano*, 2012, **6**, 2940–2947.
- 13 S.-H. Choi, H. B. Na, Y. I. Park, K. An, S. G. Kwon, Y. Jang, M.-H. Park, J. Moon, J. S. Son, I. C. Song, W. K. Moon and T. Hyeon, *J. Am. Chem. Soc.*, 2008, **130**, 15573–15580.
- 14 C. Xu, J. Xie, D. Ho, C. Wang, N. Kohler, E. G. Walsh, J. R. Morgan, Y. E. Chin and S. Sun, *Angew. Chem., Int. Ed.*, 2008, **47**, 173–176.
- 15 C. Xu, B. Wang and S. Sun, *J. Am. Chem. Soc.*, 2009, **131**, 4216–4217.
- 16 J.-S. Choi, Y.-W. Jun, S.-I. Yeon, H. C. Kim, J.-S. Shin and J. Cheon, *J. Am. Chem. Soc.*, 2006, **128**, 15982–15983.
- 17 D. V. Talapin, J. S. Lee, M. V. Kovalenko and E. V. Shevchenko, *Chem. Rev.*, 2010, **110**, 389–458.
- 18 R. E. Schaak and M. E. Williams, *ACS Nano*, 2012, **6**, 8492–8497.
- 19 L. Carbone, C. Nobile, M. De Giorgi, F. Della Sala, G. Morello, P. Pompa, M. Hytch, E. Snoeck, A. Fiore, I. R. Franchini, M. Nadasan, A. F. Silvestre, L. Chiodo, S. Kudera, R. Cingolani, R. Krahne and L. Manna, *Nano Lett.*, 2007, **7**, 2942–2950.
- 20 T. Wang, J. Zhuang, J. Lynch, O. Chen, Z. Wang, X. Wang, D. LaMontagne, H. Wu, Z. Wang and Y. C. Cao, *Science*, 2012, **338**, 358–363.

- 21 Y. Ben-Shahar, F. Scotognella, I. Kriegel, L. Moretti, G. Cerullo, E. Rabani and U. Banin, *Nat. Commun.*, 2016, **7**, 10413.
- 22 N. J. Borys, M. J. Walter, J. Huang, D. V. Talapin and J. M. Lupton, *Science*, 2010, **330**, 1371–1374.
- 23 J. Dimitrijevic, L. Krapf, C. Wolter, C. Schmidtke, J.-P. Merkl, T. Jochum, A. Kornowski, A. Schüth, A. Gebert, G. Hüttmann, T. Vossmeier and H. Weller, *Nanoscale*, 2014, **6**, 10413–10422.
- 24 H. Li, R. Brescia, R. Krahne, G. Bertoni, M. J. P. Alcocer, C. D'Andrea, F. Scotognella, F. Tassone, M. Zanella, M. De Giorgi and L. Manna, *ACS Nano*, 2012, **6**, 1637–1647.
- 25 G. Jia and U. Banin, *J. Am. Chem. Soc.*, 2014, **136**, 11121–11127.
- 26 G. Jia, A. Sitt, G. B. Hitin, I. Hadar, Y. Bekenstein, Y. Amit, I. Popov and U. Banin, *Nat. Mater.*, 2014, **13**, 301–307.
- 27 B. O. Dabbousi, J. Rodriguez Viejo, F. V. Mikulec, J. R. Heine, H. Mattoussi, R. Ober, K. F. Jensen and M. G. Bawendi, *J. Phys. Chem. B*, 1997, **110**, 9463–9475.
- 28 X. Peng, M. C. Schlamp, A. V. Kadavanich and A. P. Alivisatos, *J. Am. Chem. Soc.*, 1997, **119**, 7019–7029.
- 29 B. Ji, Y. E. Panfil, N. Waiskopf, S. Remennik, I. Popov and U. Banin, *Nat. Commun.*, 2019, **10**, 2.
- 30 M. Lomascolo, A. Creti, G. Leo, L. Vasanelli and L. Manna, *Appl. Phys. Lett.*, 2003, **82**, 418–420.
- 31 D. Chen, H. Zhang, Y. Li, Y. Pang, Z. Yin, H. Sun, L.-C. Zhang, S. Wang, M. Saunders, E. Barker and G. Jia, *Adv. Mater.*, 2018, **30**, 1803351.
- 32 A. M. Smith, A. M. Mohs and S. Nie, *Nat. Nanotechnol.*, 2009, **4**, 56–63.
- 33 C.-M. Ning, L. Dou and P. Yang, *Nat. Rev. Mater.*, 2017, **2**, 17070.
- 34 T. Mokari and U. Banin, *Chem. Mater.*, 2003, **15**, 3955–3960.
- 35 N. Oh and M. Shim, *J. Am. Chem. Soc.*, 2016, **138**, 10444–10451.
- 36 C.-Y. Yeh, Z. W. Lu, S. Froyen and A. Zunger, *Phys. Rev. B: Condens. Matter Mater. Phys.*, 1992, **46**, 10085–10097.
- 37 T. Omata, H. Uesugi and M. Kita, *J. Cryst. Growth*, 1994, **394**, 81–88.
- 38 P. D. Cozzoli, L. Manna, M. L. Curri, S. Kudera, C. Giannini, M. Striccoli and A. Agostiano, *Chem. Mater.*, 2005, **17**, 1296–1306.
- 39 W. Chen, A. Karton, T. Hussian, S. Javaid, F. Wang, Y. Pang and G. Jia, *CrystEngComm*, 2019, **13**, 2955–2961.
- 40 K. Boldt, C. Ramanan, A. Chanaewa, M. Werheid and A. Eychmüller, *J. Phys. Chem. Lett.*, 2015, **6**, 2590–2597.
- 41 K. Boldt, K. N. Schwarz, N. Kirkwood, T. A. Smith and P. Mulvaney, *J. Phys. Chem. C*, 2014, **118**, 13276–13284.
- 42 D. Dorfs, A. Salant, I. Popov and U. Banin, *Small*, 2008, **4**, 1319–1323.
- 43 D. H. Son, S. M. Hughes, Y. Yin and A. P. Alivisatos, *Science*, 2004, **306**, 1009–1012.
- 44 W. Li, R. Zamani, M. Ibáñez, D. Cadavid, A. Shavel, J. R. Morante, J. Arbiol and A. Cabot, *J. Am. Chem. Soc.*, 2013, **135**, 4664–4667.
- 45 L. De Trizio and L. Manna, *Chem. Rev.*, 2016, **116**, 10852–10887.
- 46 H. Du, C. Chen, R. Krishnan, T. D. Krauss, J. M. Harbold, F. W. Wise, M. G. Thomas and J. Silcox, *Nano Lett.*, 2002, **2**, 1321–1324.
- 47 V. V. Rossin, T. Böttger and F. Henneberger, *Phys. Rev. B: Condens. Matter Mater. Phys.*, 1996, **54**, 7682.

Supporting Information

Colloidal Quasi-One-Dimensional Dual Semiconductor Core/Shell Nanorod Couple Heterostructures with Blue Fluorescence

*Dechao Chen, Aixiang Wang, Hongbo Li, Laura Abad Galán, Cong Su, Zongyou Yin,
Massimiliano Massi, Alexandra Suvorova, Martin Saunders, Ju Li, Amit Sitt,* Guohua Jia**

Experimental Section

Chemicals: $\text{Zn}(\text{NO}_3)_2 \cdot 6\text{H}_2\text{O}$ (99%), zinc diethyldithiocarbamate (97%), selenium powder (99.999%), CdO (99%), sulfur (99%), bis(trimethylsilyl)sulfide (98%), dodecanethiol (98%), oleylamine (approximate C_{18} content 80–90%), oleic acid (90%, technical grade), 1-octadecene (90%, technical grade), trioctylphosphine (TOP, 97%), trioctylphosphine oxide (TOPO, 90%), toluene (99.8%, anhydrous), chloroform (99%, anhydrous), and methanol (99.8% anhydrous) were purchased from Sigma-Aldrich. Octadecylphosphonic acid (ODPA) and hexylphosphonic acid (HPA) were purchased from PCI Synthesis. All chemicals were used as received without further purification.

Preparation of Zinc Precursor Stock Solution: A 0.067 M zinc stock solution was prepared by dissolved $\text{Zn}(\text{NO}_3)_2 \cdot 6\text{H}_2\text{O}$ (0.2 mmol) in oleylamine (10 mL) in a three-neck flask. The mixture was degassed and refilled with N_2 three times at room temperature and then heated to 110 °C and kept at this temperature under vacuum for 30 minutes. Then the mixture was further heated up to 160 °C and kept at this temperature for 30 minutes.

Synthesis of thin ZnSe nanorods: Thin ZnSe nanorods synthesis was conducted according to a previously reported approach with some modifications.²⁶ In a typical synthesis, 0.2 mmol (59.5 mg) $\text{Zn}(\text{NO}_3)_2 \cdot 6\text{H}_2\text{O}$ and 10 mL oleylamine were mixed in a three-neck flask. The mixture was degassed and refilled with N_2 three times at room temperature and then heated to 110 °C and kept at this temperature for 0.5 hour. At 160 °C, 2 mL 0.1 M Se oleylamine solution was injected into the flask. After the injection, the temperature was set at 120 °C and the mixture was degassed for 10 minutes. After the flask was refilled with N_2 , the temperature was raised up to 230 °C in 6 minutes. After 20 minutes at 230 °C, the reaction was quenched by removing the heating mantle.

Purification of thin ZnSe nanorods: Purification of nanoparticles was conducted by dissolving 2 mL of the crude solution into 2 mL chloroform solution. Then methanol was continuously added into the solution until a turbid solution was obtained. The precipitation was separated from the solution by the aid of centrifugation and this procedure may repeat two or three times.

Synthesis of hetero- ZnS-ZnSe/ZnS core/shell Nanorod Couples: 30 mg purified thin ZnSe nanorods were dissolved in 15 mL oleylamine in a three-neck flask and then 4 mL 0.067 M zinc precursor stock solution was added into the flask. The mixture was degassed and refilled with N₂ three times at room temperature and then heated to 110 °C and kept at this temperature for 30 minutes under vacuum. Then the mixture was heated to 260 °C in 7 minutes. At 260 °C, 1 mL (4.17 mmol) of 1-dodecanethiol was injected into the flask. After the injection, the temperature was raised to 280 °C in four minutes. After 30 minutes at 280 °C, the reaction was quenched by removing the heating mantle. Aliquots have been taken from time to time to monitor the growth of nanoparticles. Other sulfur source, such as (4.0 mmol) bis(trimethylsilyl)sulfide, has been used to substitute 1-dodecanethiol for synthesis of branched nanorod couples. The synthetic conditions for the synthesis of hetero- ZnS-ZnSe/ZnS core/shell nanorod couples using bis(trimethylsilyl)sulfide as the sulfur source are exactly same as above except 1-dodecanethiol has been replaced by bis(trimethylsilyl)sulfide.

Synthesis of homo- ZnSe Nanorod Couples: The synthesis of homo- ZnSe nanorod couples was conducted according to a previously reported approach with some modifications.²⁶ In a typical synthesis, 30 mg purified thin ZnSe nanorods was dissolved into 15 mL oleylamine solution into a three-neck flask. 1 mL 0.067 M zinc oleylamine and 1 mL 0.067 M selenium oleylamine stock solutions were added the flask at room temperature. Then the reaction solution was gradually heated up to 280 °C in 15 minutes and kept at this

temperature for 30 minutes. The reaction was quenched by removing the heating mantle. Aliquots have been taken from time to time to monitor the growth of nanoparticles.

Etching of ZnSe Nanorods: 30 mg purified thin ZnSe nanorods were synthesized by a reported approach^{26,44} and were dissolved in 15 mL oleylamine in a three-neck flask and then 4 mL 0.067 M zinc precursor stock solution was added into the flask. The mixture was degassed and refilled with N₂ three times at room temperature for three times and then heated to 110 °C and kept at this temperature for 30 minutes under vacuum. Then the mixture was heated to 260 °C in 7 minutes. At 260 °C, a certain amount of 1-dodecanethiol was injected into the flask. After the injection, the temperature was raised to 280 °C in four minutes. After 30 minutes at 280 °C, the reaction was quenched by removing the heating mantle. Aliquots have been taken from time to time to evolution of the nanoparticles.

Synthesis of ZnSe/ZnCdS Core/Shell Nanorod Couples: For the CdS shell growth, CdO (15 mg), trioctylphosphine oxide (2.0 g), octadecylphosphonic acid (75 mg) and hexylphosphonic acid (10 mg) were added to a three-neck flask (50 ml). The mixture was heated to 150 °C for 0.5 h under vacuum and then rise to 320 °C at N₂ to obtain a colourless solution. After that, the mixture was heated and stabilized at 365 °C and 3 ml TOP solution dissolved with 1×10^{-9} mol branched hetero- ZnS-ZnSe nanorod couples and 30mg sulfur was swiftly injected into the flask. After 30 seconds, the reaction was quenched by ice bathing. The crude reaction solution was diluted with toluene, methanol was added to precipitate the nanocrystals and remove excess surfactants.

Synthesis of Branched Hetero- PbS-PbSe Nanorod Couples: The cation exchange method was used to obtain branched hetero- PbS-PbSe nanorod couples from branched hetero- ZnS-ZnSe nanorod couples. A 0.05 M lead oleate stock solution was prepared by dissolving lead acetate (1 mmol) in a mixture of oleic acid (0.88 ml) and octadecene (19.12

ml) at 180 °C. The purified branched hetero- ZnS-ZnSe nanorod couples was dissolved in 1 mL anhydrous chloroform and then injected into 5 ml oleylamine in a 15 ml three-neck flask. After place in vacuum for 10 min, lead oleate stock (0.05 M) solution was injected into the flask and the temperature was raised to 100°C. After 5min at this temperature, the colorless solution transformed to dark brown, which indicates the Zn²⁺ ions have been substituted by Pb²⁺. The solution was quenched by ice bathing and the obtained solution was washed by toluene and precipitated by methanol with the aid of centrifugation.

Synthesis of CdS rods: CdS nanorods were prepared using a literature method.¹ In a typical synthesis, CdO (60 mg), trioctylphosphine oxide (3.0 g), octadecylphosphonic acid (290 mg) and hexylphosphonic acid (45 mg) were added to a three-neck flask (50 ml). The mixture was heated to 150 °C for 0.5 h under vacuum and then rise to 320 °C at N₂ to obtain a colourless solution. After that, the mixture was heated and stabilized at 365 °C and 1.8 ml TOP solution dissolved with 4×10⁻⁸ mol CdS spherical dots and 60 mg sulfur was swiftly injected into the flask. After 9 minutes, the reaction was quenched by ice bathing. The crude reaction solution was diluted with toluene, methanol was added to precipitate the nanocrystals and remove excess surfactants with the aid of centrifugation.

Sample Characterization.

UV-vis Absorption Spectroscopy: UV-vis absorption spectroscopy was performed on a Perkin Elmer Lambda 35 UV/VIS Spectrometer using quartz cuvettes.

Photophysical measurements: Uncorrected steady-state emission spectra were recorded using an Edinburgh FLSP980-stm spectrometer equipped with a 450 W xenon arc lamp, double excitation and emission monochromators, a Peltier-cooled Hamamatsu R928P photomultiplier (185-850 nm). Emission spectra were corrected for source intensity (lamp and grating) and emission spectral response (detector and grating) by a calibration curve supplied with the

instrument. Overall quantum yields were measured with the use of an integrating sphere coated with BenFlect. Fluorescence emission lifetimes (τ) were determined with the time-correlated single photon counting technique (TCSPC) with the same Edinburgh FLSP920 spectrometer using pulsed picosecond LEDs (ELED 280 or ELED 320, FWHM <800 ps) as the excitation source, with repetition rates between 10 kHz and 1 MHz, and the above-mentioned R928P PMT as detector. To record the fluorescence spectra at 77 K, the samples were placed in quartz tubes (2 mm diameter) and inserted in a special quartz Dewar filled with liquid nitrogen. To measure the fluorescence spectra at different temperatures from 77 K to 287 K, the samples were placed in quartz cuvettes in a liquid nitrogen cryostat (Oxford Instrument). All the solvents used in the preparation of the solutions for the photophysical investigations were of spectrometric grade. Experimental uncertainties are estimated to be $\pm 10\%$ for lifetimes and $\pm 20\%$ for quantum yields.

XRD Measurement: XRD patterns were obtained using Cu K α ($\lambda=1.5406$ Å) photons from an X'per PRO (PANalytical) X-ray diffractometer operated at 40 kV and 40 mA. Samples were deposited as a thin layer on a low-background scattering quartz substrate.

TEM Measurement: TEM grids were prepared by depositing one drop of a solution of purified nanoparticles onto a standard carbon coated grid. TEM was performed using a JEOL 2100 transmission electron microscope with a tungsten filament running at an accelerating voltage of 120 keV. HRTEM, HAADF-STEM, High-resolution Z-contrast STEM and STEM-energy-dispersive X-ray spectroscopy (EDX) were performed on an FEI Titan G2 80-200 high-resolution transmission electron microscope running at an accelerating voltage of 200 keV with a field emission gun as an electron source.

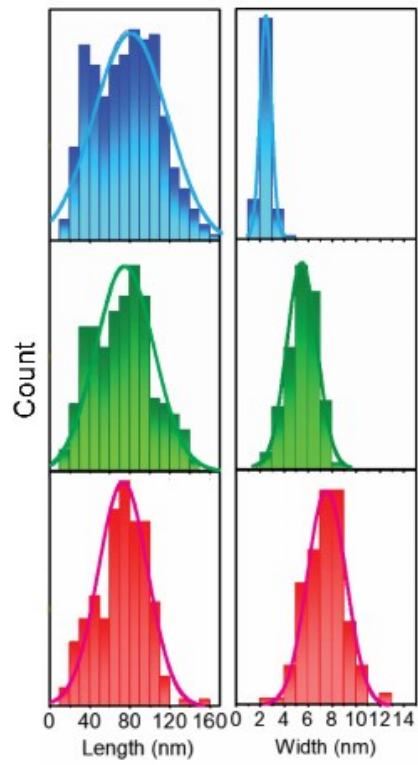


Figure S1. Sizing histograms of original ZnSe nanorods (top panel), hetero- ZnS-ZnSe/ZnS nanorod couples obtained after 30 seconds at 280 °C (middle panel), and branched hetero-ZnS-ZnSe/ZnS nanorod couples obtained after 30 minutes at 280 °C (bottom panel).

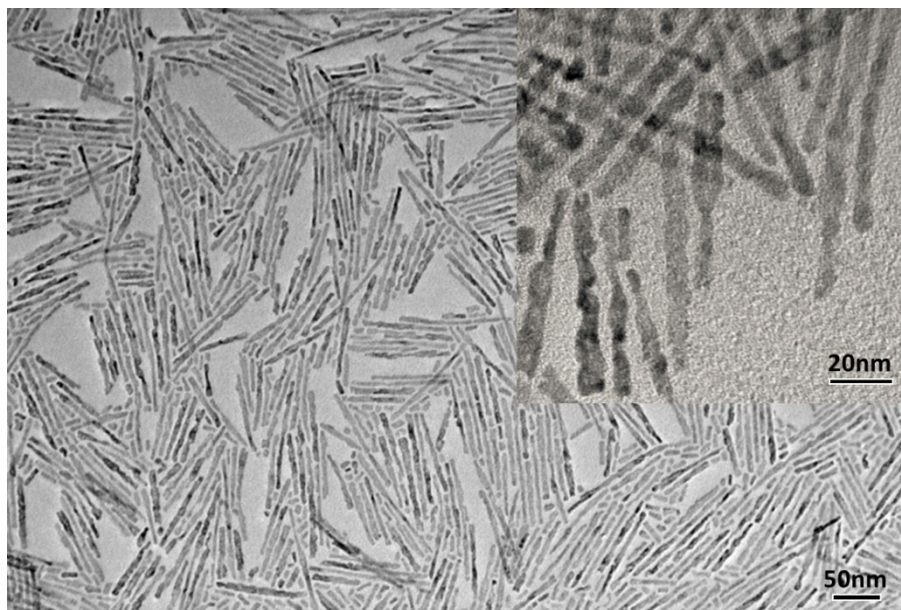


Figure S2. TEM image of hetero- ZnS-ZnSe/ZnS core/shell nanorod couples synthesized using bis(trimethylsilyl)sulfide as the sulfur source. Inset show a zoom-in of nanoparticles.

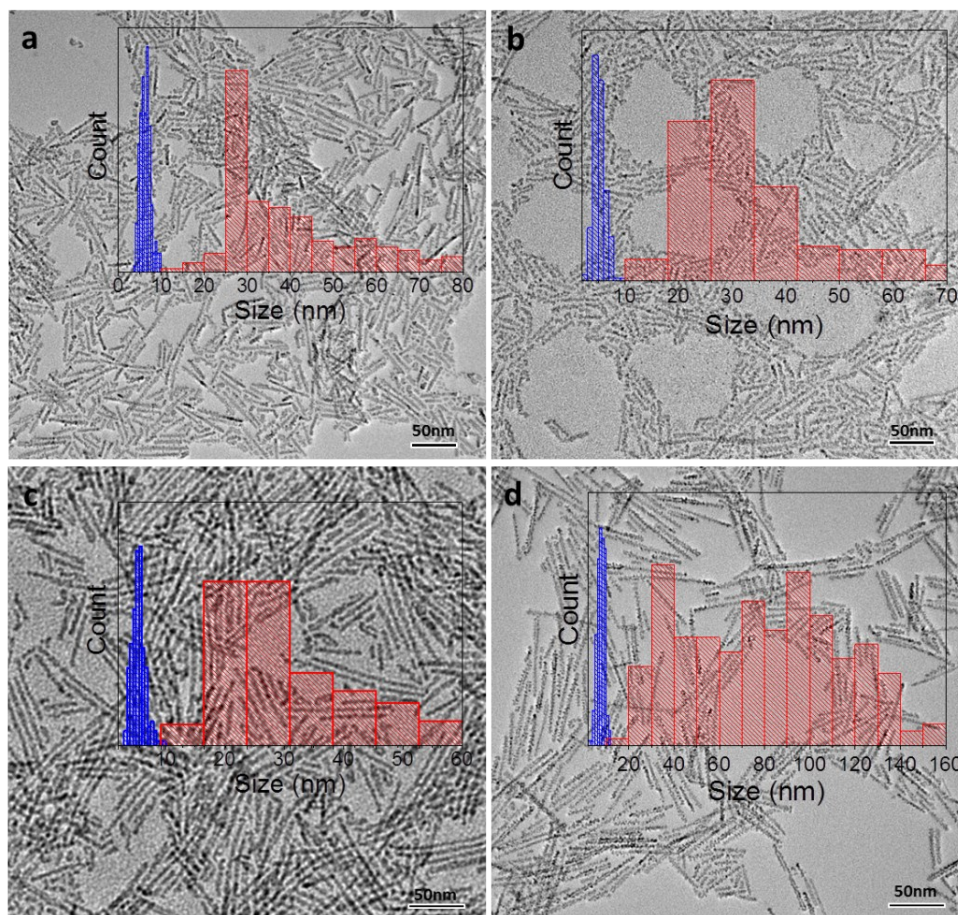


Figure S3. TEM images and sizing histograms of branched hetero- ZnS-ZnSe/ZnS nanorod couples with different dimensions. (a) Length (42.3 ± 17.9 nm) \times width (6.3 ± 1.2 nm). (b) Length (37.7 ± 20.5 nm) \times width (5.3 ± 1.1 nm). (c) Length (45.1 ± 23.4 nm) \times width (5.4 ± 1.1 nm). (d) Length (79.6 ± 35.2 nm) \times width (7.7 ± 1.6 nm).

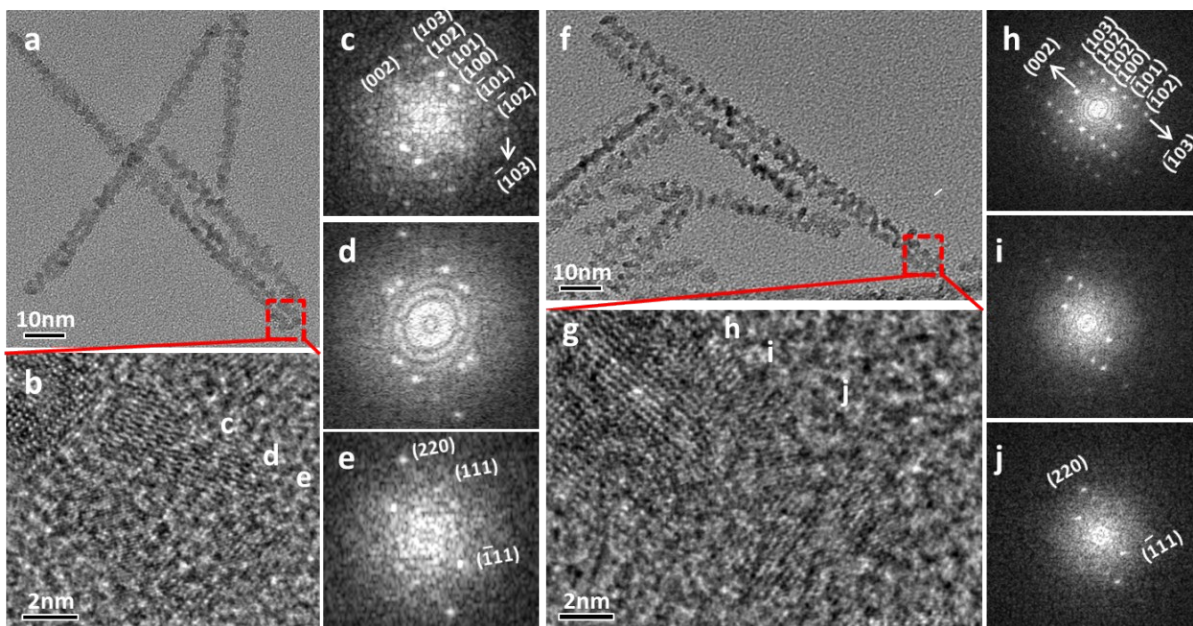


Figure S4. Electron microscopy imaging characterizations of hetero- ZnS-ZnSe/ZnS core/shell nanorod couples. (a) TEM image. (b) HRTEM image of the short arm labelled by dashed rectangle in (a), showing a hetero- nanorod couple is formed by the growth of zincblende ZnS between the end facets of two parallelly aligned wurtzite ZnSe nanorods. (c-e) FFT of selected areas in (b) revealing the crystallographic relations. The diffraction patterns in (c) and (e) match wurtzite ZnSe and zincblende ZnS, respectively. (d) shows the concurrence of above two sets of diffraction patterns. (f) TEM image. (g) HRTEM image of the short arm labelled by dashed rectangle in (f). (h-i) FFT of selected areas in (g) revealing the crystallographic relations. The diffraction patterns in (h) and (j) match wurtzite ZnSe and zincblende ZnS, respectively.

Table S1. Comparison of lattice mismatches of the nanostructures.

Initial material	(0002) wurtzite ZnSe	(0002) wurtzite ZnSe	(0002) wurtzite ZnSe
Second material	(111) zinblende ZnS	(0002) wurtzite ZnS	(0002) wurtzite CdS
Mismatch (%)	3.9 ³	4.5 ⁴	3.4 ^{5,6}

The mismatches were calculated by the equation below:

Lattice mismatch = (lattice parameter of initial material – lattice parameter of a second material)/ lattice parameter of initial material.

The lattice plane spacings for (0002) of wurtzite ZnSe, (111) of zinblende ZnS, (0002) of wurtzite ZnS and (0002) of wurtzite CdS are 0.32500 nm, 0.3123 nm, 0.31292 nm and 0.33599 nm, respectively.

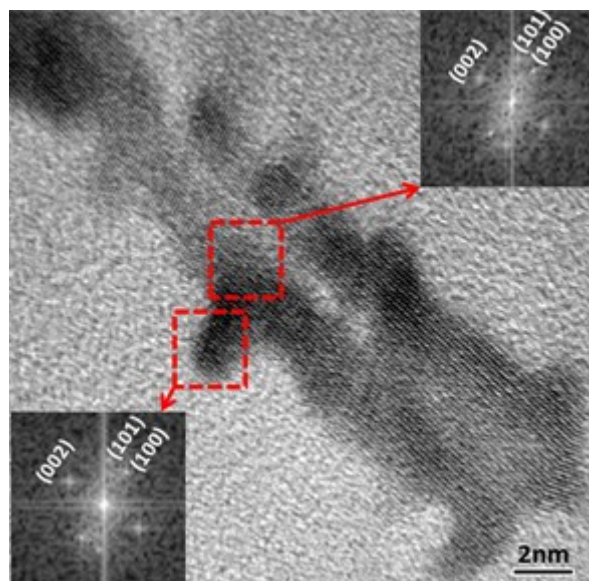


Figure S5. TEM images of “dual” nanorods showing the gap between two rod components. Insets show the FFT analyses of the selected areas.

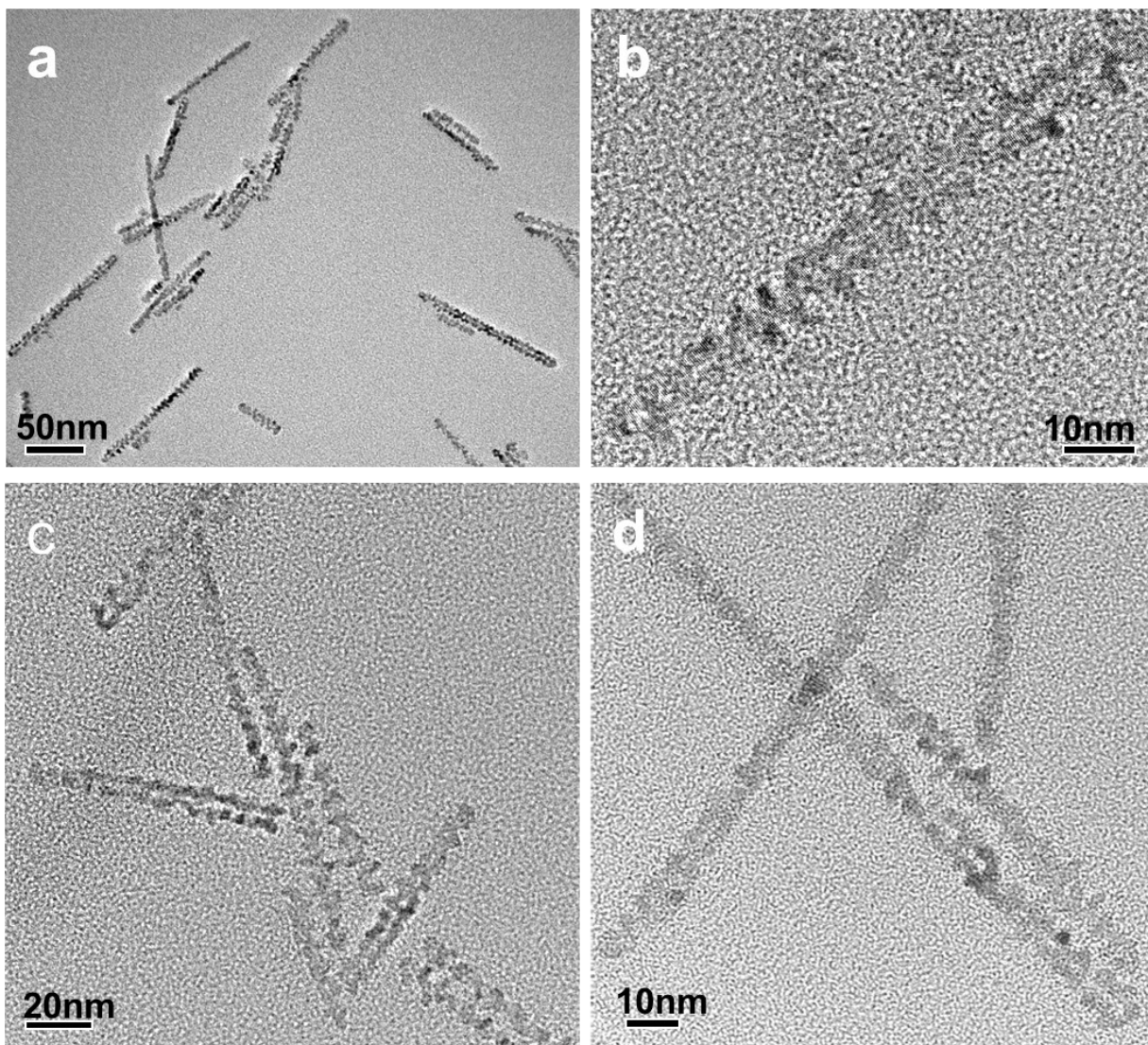


Figure S6. TEM images of hetero- ZnS-ZnSe/ZnS nanorod couples showing the gap between two rod components.

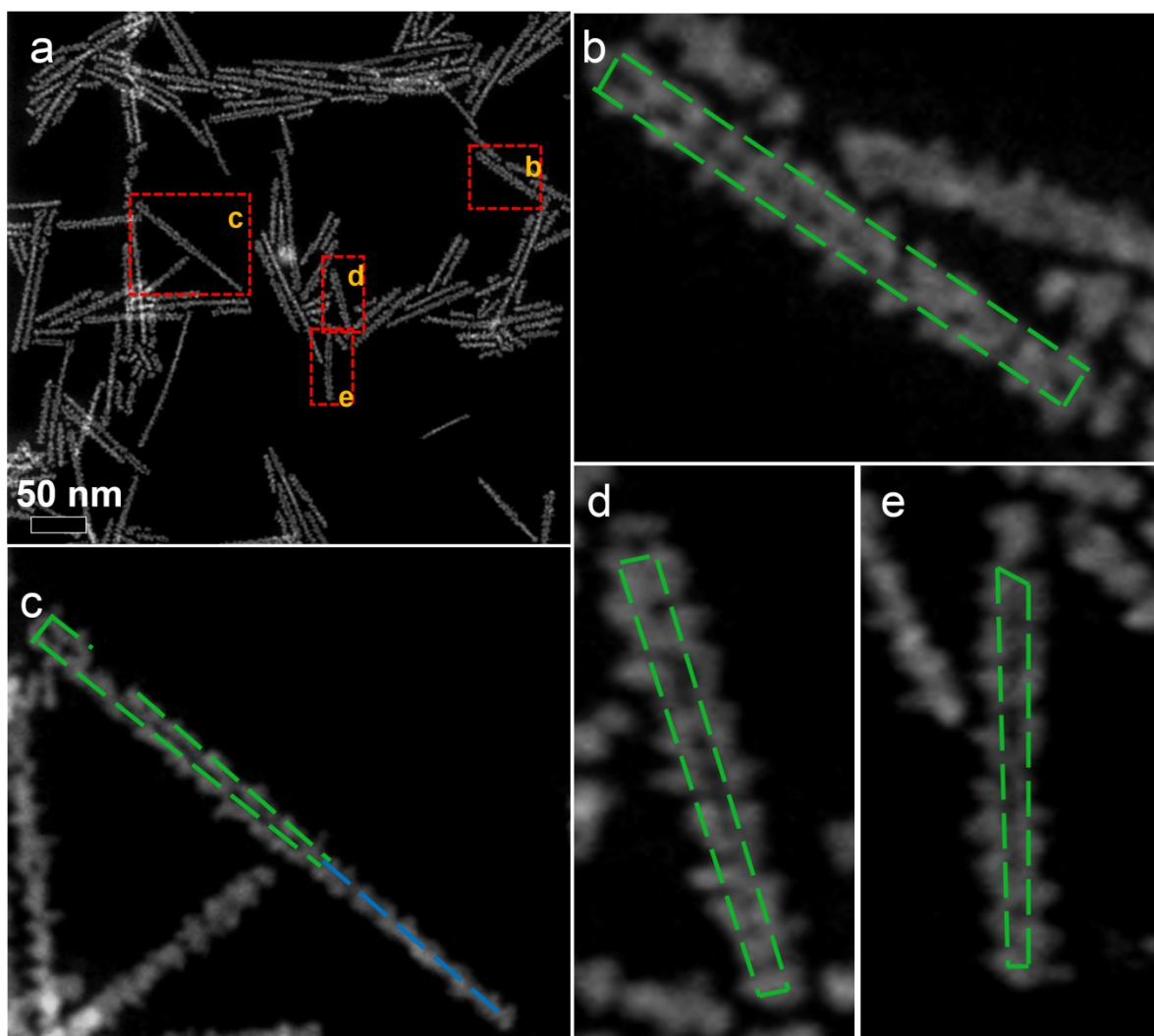


Figure S7. HAADF-STEM images showing the gap between two rod components of hetero- ZnS- ZnSe/ZnS nanorod couples. (a) Branched hetero- nanorod couples. (b-e) Enlarged images of individual nanoparticle as marked by red rectangles in (a). The green lines outline the long rod components, and blue line indicates single rod features of a branched nanorod couple which was formed due to partial coalesce of side facet of the “dual rods” occurred at elevated temperatures, e.g. 280 °C.

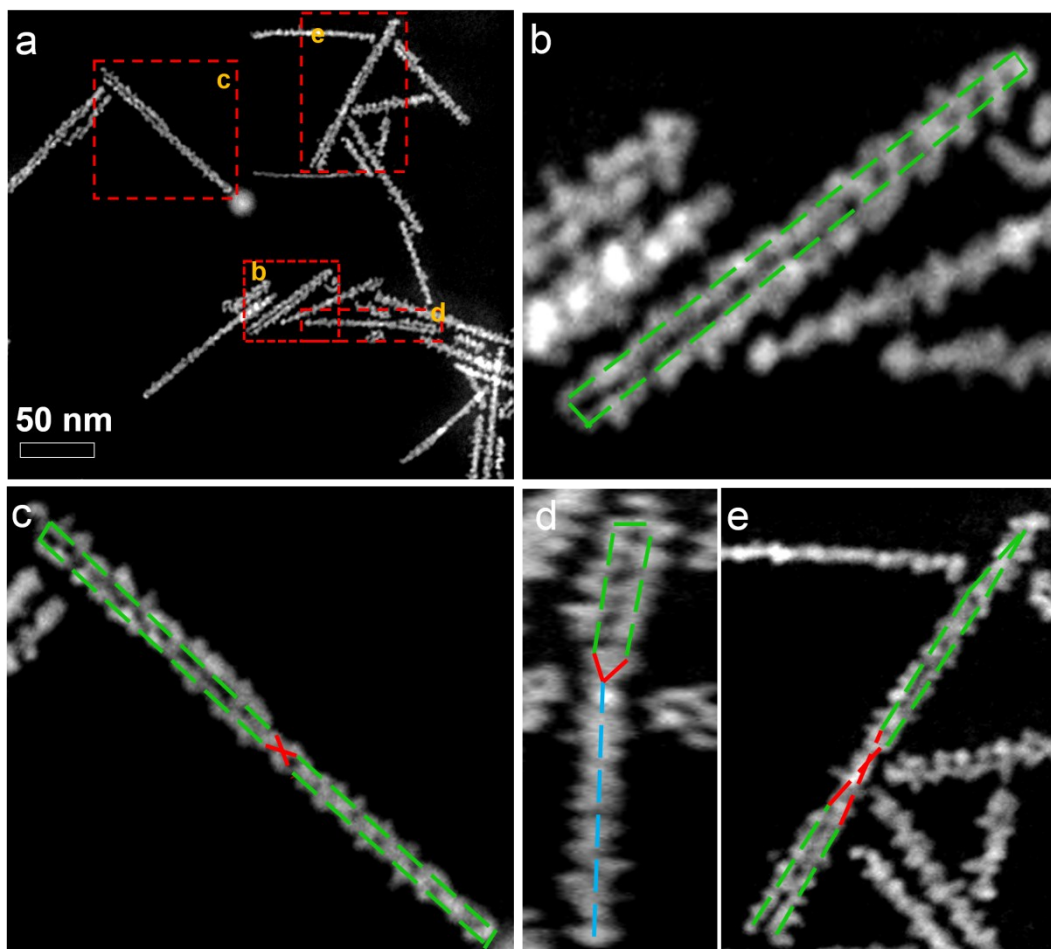


Figure S8. HAADF-STEM images of a) branched hetero- nanorod couples. b,c,d,e) Enlarged images of particles marked by red rectangles in a). The green lines outline the long rod components, and blue line indicates single rod features of a branched nanorod couple, and the red cross indicates the twist features of branched nanorod couples.

In general, the features of branched nanorod couples can be recognized with the guide of the green lines marked in the enlarged HAADF-STEM images. It is evident that the majority of branched nanorod couples remains the “dual rods” features. In Figure S7c and S8d, some parts of branched nanorods couples show single rod feature because of the partial coalesce of side facet of the “dual rods” occurred at elevated temperatures, e.g. 280 °C. Other branched nanorods couples also show twisting, as marked by red cross, which is also observed in the previously reported ZnSe nanorod couples.²

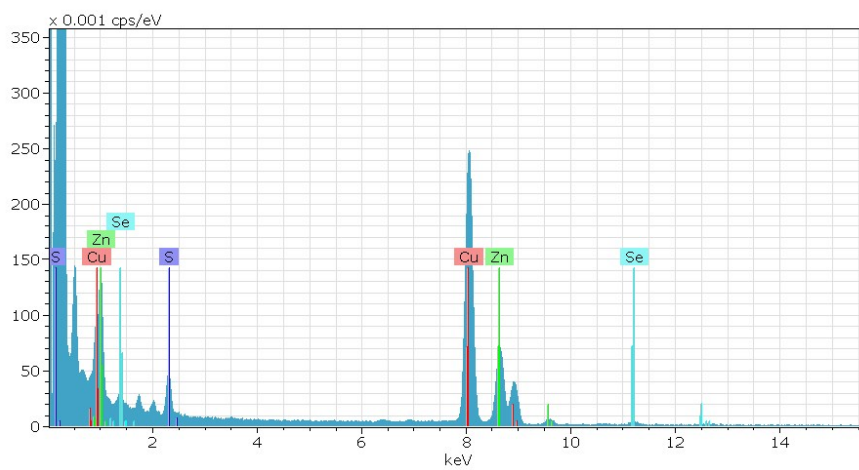


Figure S9. EDX spectrum of branched hetero- ZnS-ZnSe/ZnS core/shell nanorod couples confirming the presence of Zn, Se and S elements.

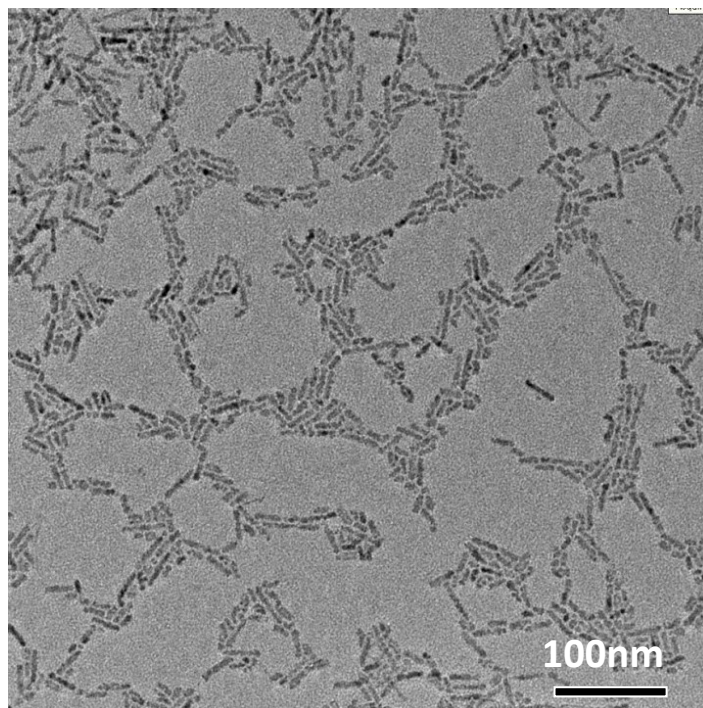


Figure S10. TEM images of etched ZnSe nanorod with rough surface facets obtained in oleylamine solution in the presence of 1-dodecanethiol after the reaction evolved for 30 minutes at 280 °C.

Electronic structure calculation

A finite well effective mass approximation (EMA) approach⁷ was used to study the electronic structure of the hetero-ZnSe-ZnS/ZnSe core/shell nanorod couples, and in particular to compare them to that of homo- ZnSe nanorod couples. Due to the complex shape of the system, the solution was performed numerically using a finite element based model obtained with COMSOL Multiphysics package.

Within the EMA, we modeled the excited charge carrier confined to the particle as a particle in a box. Under this approximation, the Schrödinger equation for the electron (hole) envelope wave functions, φ_a , is defined as

$$\left(-\frac{\hbar}{2m_a^*} \nabla^2 + V_a \right) \varphi_a = E_a \varphi_a, \quad a = e/h \quad (1)$$

where \hbar is the reduced Planck constant, m_a^* is the reduced mass and V_a is the potential energy exerted on the charge carrier in the medium.

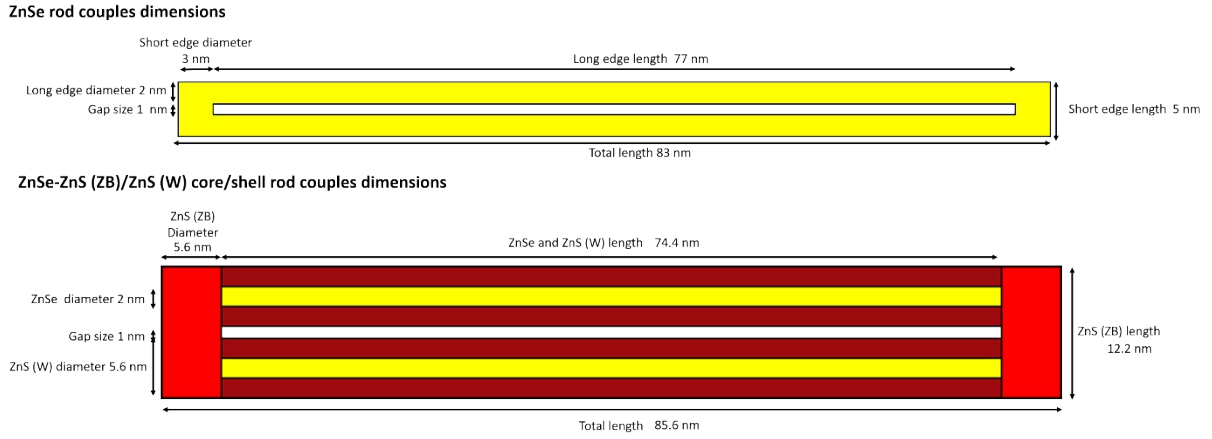
The total exciton energy can be calculated by

$$E = E_{bg} + E_e + E_h \quad (2)$$

where E_{bg} is the bulk's band gap. The potential energy of the charge carriers within the particle is taken as zero. The potential energy outside the particle, which determines the height of the well's wall, was set to $V_{ligands} = [E_{LH}(ligands) - E_{bg}(ZnSe)]/2$, where $E_{LH}(ligands)$ is the energy difference between the LUMO and HOMO energies of the ligand. For oleylamine, $E_{LH}(ligands) = 4.430 \text{ eV}$.⁸

In this calculations, Coulomb, Exchange, and Correlation interactions were neglected as they were not easily obtained for elongated systems, and may further shift the exciton's energy. We took both the bulk band gap energy for ZnSe and ZnS and the effective masses from references⁹⁻¹³, and are summarized in Table S2. The hole states correspond to the heavy hole, which dominates the valence band-edge states in this system.

Comparison between the electronic structure of hetero-ZnSe-ZnS/ZnS nanorod couples and homo- ZnSe was obtained for systems of similar ZnSe dimensions. All geometric parameters were



Scheme S1: Dimensions of the different systems used for calculating the electronic structures set according to the dimensions extracted from TEM images and are shown in Scheme S1. The particles were embedded in an environment of organic material, with wave functions set to zero at the boundaries. The environment dimensions were increased until the difference in eigenvalues was lower than 10^{-4} eV, omitting boundary artifacts on the solution. The energies and the contour of the wave functions cross section along the zx plane were shown in Figure 4 in the main article.

As discussed in the main article, in ZnSe nanorod couples, the wavefunctions of the lowest electron/hole states reside in the corners and hence occupy the short vertices, while in the hetero-ZnS-ZnSe nanorod couples they reside in the long vertices. In the hetero-ZnS-ZnSe system, in the first 6 states, the hole and electron occupies only ZnSe rod states. Interestingly, despite lying at the edge of the conduction-band offset of ZnSe and ZnS (ZB), the electron also occupies ZnSe rod states, and this is because the first allowed state of the ZnS in the short edges has a much higher energy because of the confinement. However, the electron wavefunction penetrates the ZnS (W) shell quite significantly. Within the first 6 states, in the ZnSe there are several transitions that are well-defined because of the short/long edges states. In contrary, in the hetero-ZnS-ZnSe system, the states are almost degenerate because they are "rod" states. This difference can not be distinguished for the ensemble at room temperature but might be visible for single particles.

It should be noted that the model described above produces only a first approximation for the accurate energy values. In order to provide a more detailed picture of the electronic structure, including hole state mixing, electronic fine structure, and dipole moment induced effects, a more complex modeling is required, which is beyond the scope of the calculation described above.

Table S2. Bulk band gap energy and effective masses for ZnSe and ZnS

	ZnSe	ZnS (ZB)	ZnS (W)	Environment
m_e^*	$0.21 m_e$	$0.22 m_e$	$0.22 m_e$	$1 m_e$
m_{hh}^*	$0.67 m_e$	$1.76 m_e$	$1.4 m_e$	$1 m_e$
E_{bg}	2.82 eV	3.78 eV	3.91 eV	4.430 eV
V_e	0	0.51	0.56	0.7965 eV
V_h	0	0.45	0.53	0.7965 eV

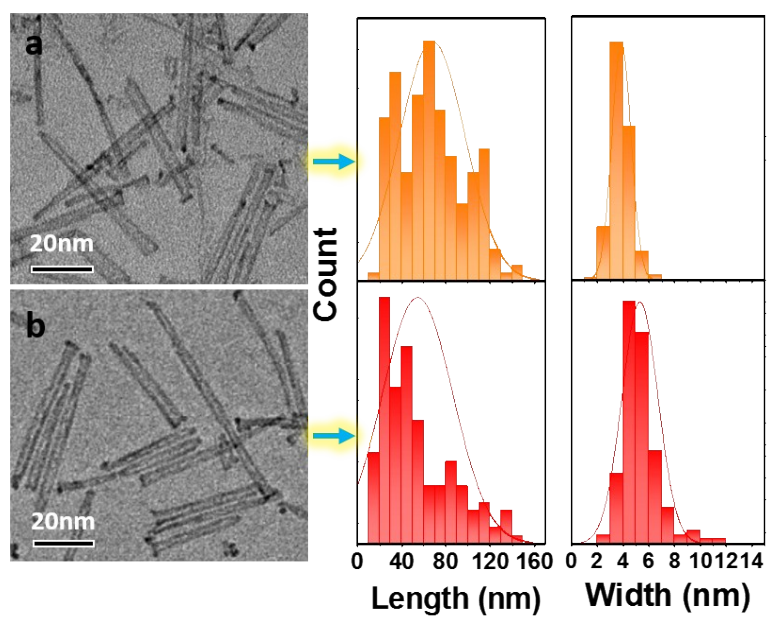


Figure S11. Sizing histograms of a) the original ZnSe nanorod couples before (top panel) (length 65.55 ± 25.40 nm \times width 6.36 ± 1.54 nm) and b) after CdS shell growth (bottom panel) (length 51.90 ± 19.30 nm \times width 7.55 ± 1.42 nm).

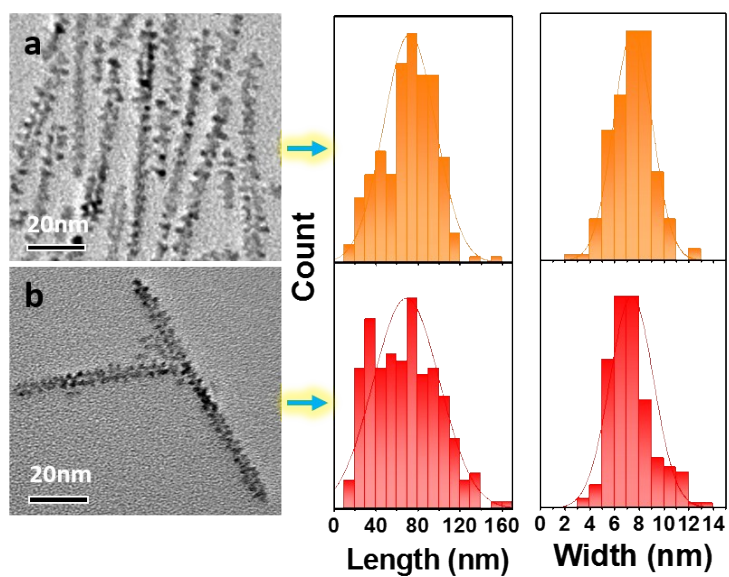


Figure S12. Sizing histograms of a) the original branched hetero- ZnS-ZnSe/ZnS nanorod couples before (top panel) (length 88.58 ± 26.93 nm \times width 7.47 ± 1.55 nm) and b) after CdS shell growth (bottom panel) (length 83.51 ± 28.50 nm \times width 7.51 ± 2.71 nm).

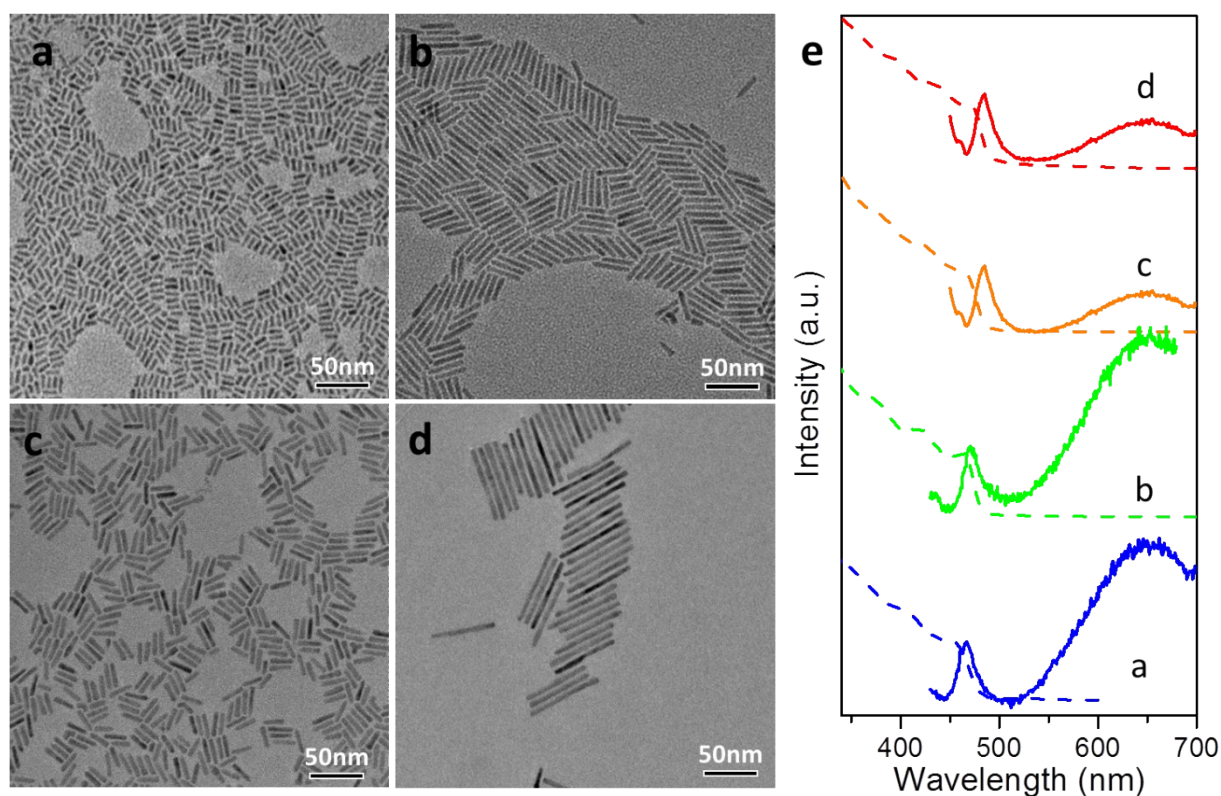


Figure S13. TEM images of CdS nanorods synthesized in TOP/TOPO using hexylphosphonic acid as the surfactant. (a-d) TEM images of CdS nanorods. (a) 3.8 nm (width) \times 11 nm (length). (b) 4.5 nm (width) \times 32 nm (length). (c) 5.5 nm (width) \times 23 nm (length). (d) 4.7 nm (width) \times 72 nm (length). (e) Absorption (dashed line) and luminescence (solid line) of CdS nanorods.

To further elucidate the origin of the blue emission of hetero- ZnS-ZnSe/ZnS/CdS core/shell/shell nanorods couples, a control experiment for the synthesis of CdS nanorods was conducted using similar synthetic conditions as those for the CdS shell growth on the ZnSe nanoparticle. All obtained CdS nanorods show a very weak band edge emission in the range of 460 nm to 476 nm and a broad band trap state emission at longer wavelengths with the luminescence quantum efficiency less than 0.1%.

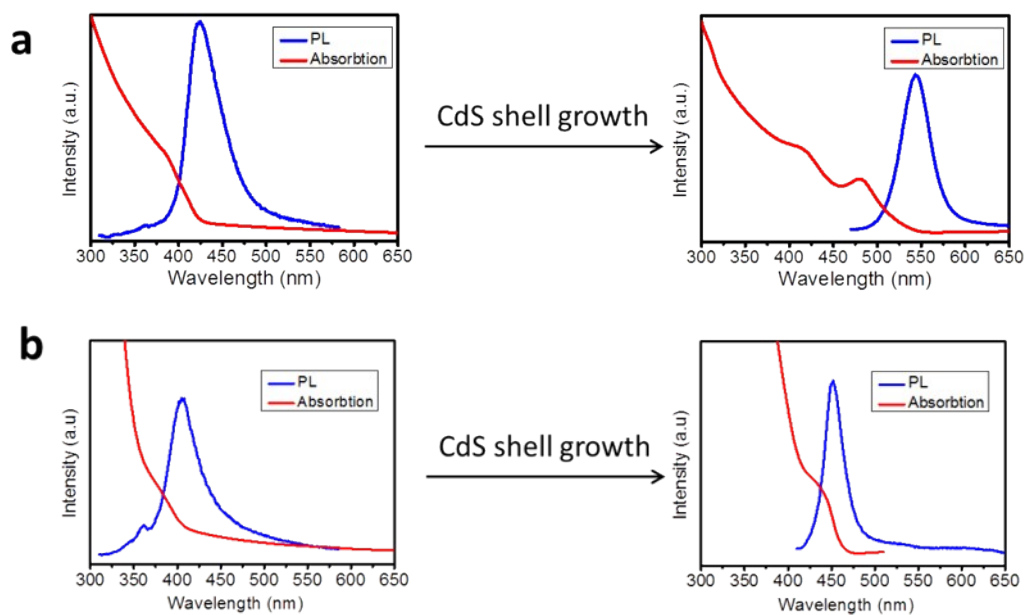


Figure S14. Comparison of absorption and luminescence spectra of nanorod couples before and after CdS shell growth. (a) Homo- ZnSe/CdS core/shell nanorod couples. (b) Hetero- ZnS-ZnSe/ZnCdS core/shell/shell nanorod couples.

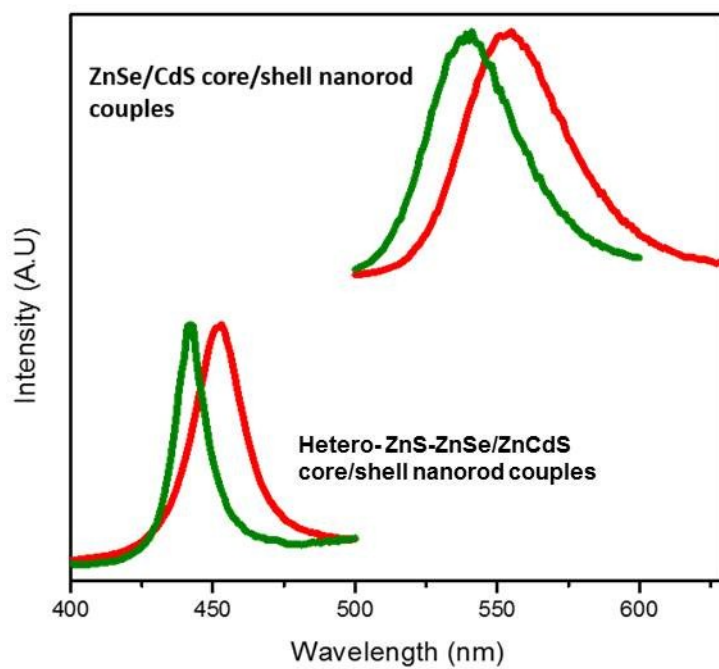


Figure S15. PL spectra of nanorods couples with the CdS shell at room temperature (red curves) and 77K (green curves).

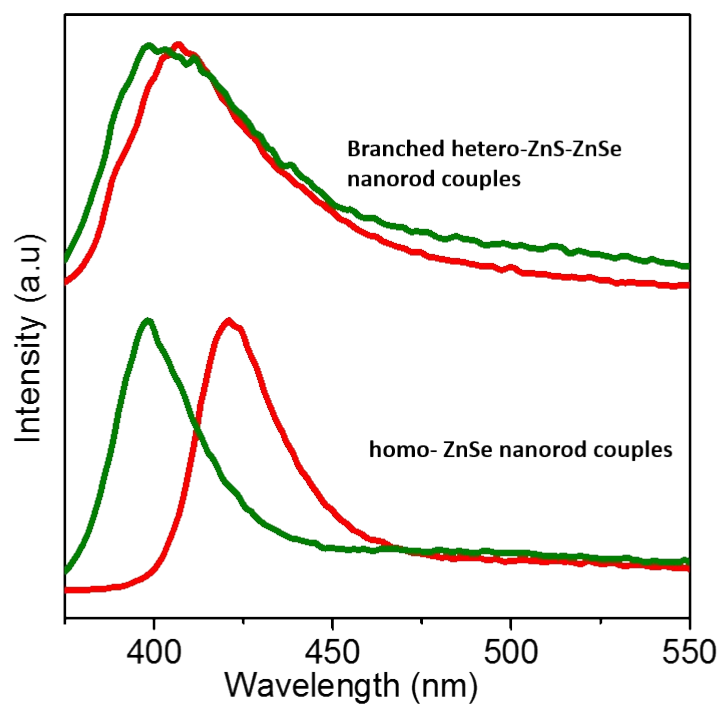


Fig S16. PL spectra of nanorods couples after surface ligand exchange with TOP at room temperature (red curves) and 77K (green curves).

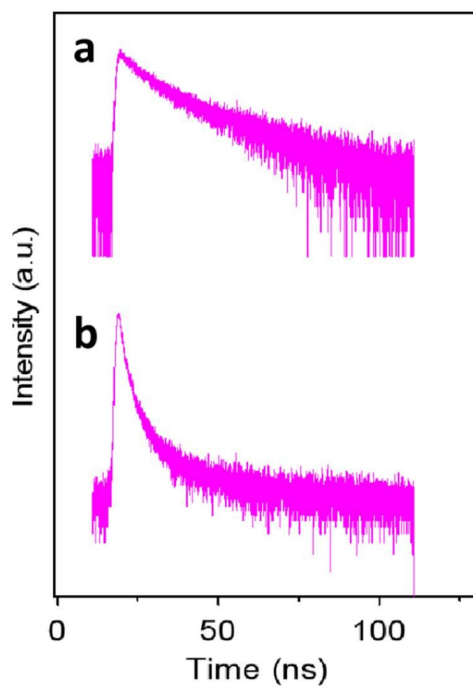


Figure S17. Comparison of 77 K fluorescence lifetime decay curves of hetero-ZnS-ZnSe/ZnCdS and homo- ZnSe/CdS core/shell nanorod couples.

Table S3 Comparison of optical properties of core/shell nanorod couples.

With CdS Shell	Emission (nm)	τ_1 (ns)	τ_2 (ns)	τ_1 percentage	Quantum Yields (%)
Hetero- nanorod couples (RT)	453	6.0	45.3	8%	2.3
Hetero- nanorod couples (77K)	442	2.5	12.1	46%	-
Homo- nanorod couples (RT)	554	10.3	50.5	20%	15.4
Homo- nanorod couples (77K)	540	7.3	32.4	18%	-

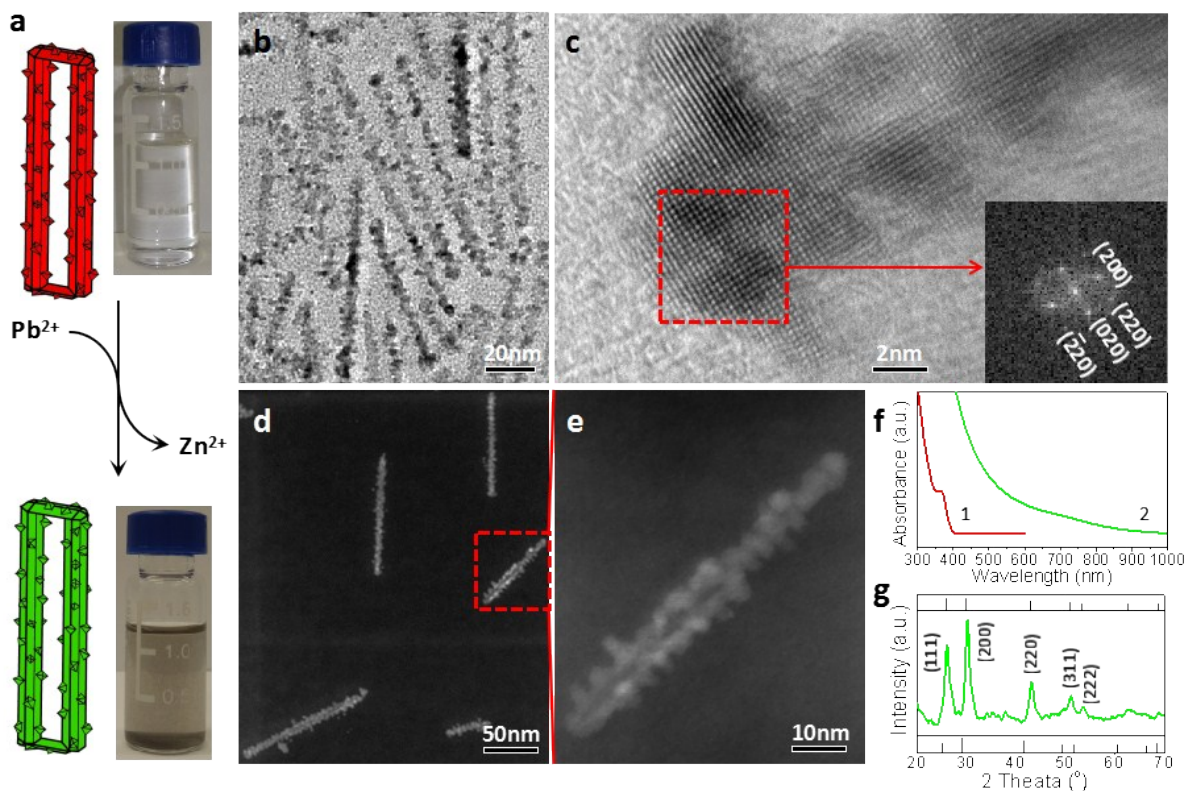


Figure S18. Branched hetero- PbS-PbSe/PbS nanorod couples obtained by a cation exchange reaction. (a) Schematic illustration of branched hetero- PbS-PbSe nanorod couples generated through Zn^{2+} replacement by Pb^{2+} . Band gap tuning is visualized by the color change of nanoparticle solutions before and after the cation exchange. (b) TEM image (c) HRTEM image. Inset in (c) shows the FFT of a selected area labelled by a red rectangle. (d,e) HAADF-STEM images of branched hetero- PbS-PbSe nanorod couples. (f) Comparison of optical absorption spectra of the branched hetero- PbS-PbSe nanorod couples before and after the cation exchange. (g) XRD patterns of branched hetero- PbS-PbSe nanorod couples. The standard XRD patterns for PbSe (bottom) and PbS (top) are given for reference.

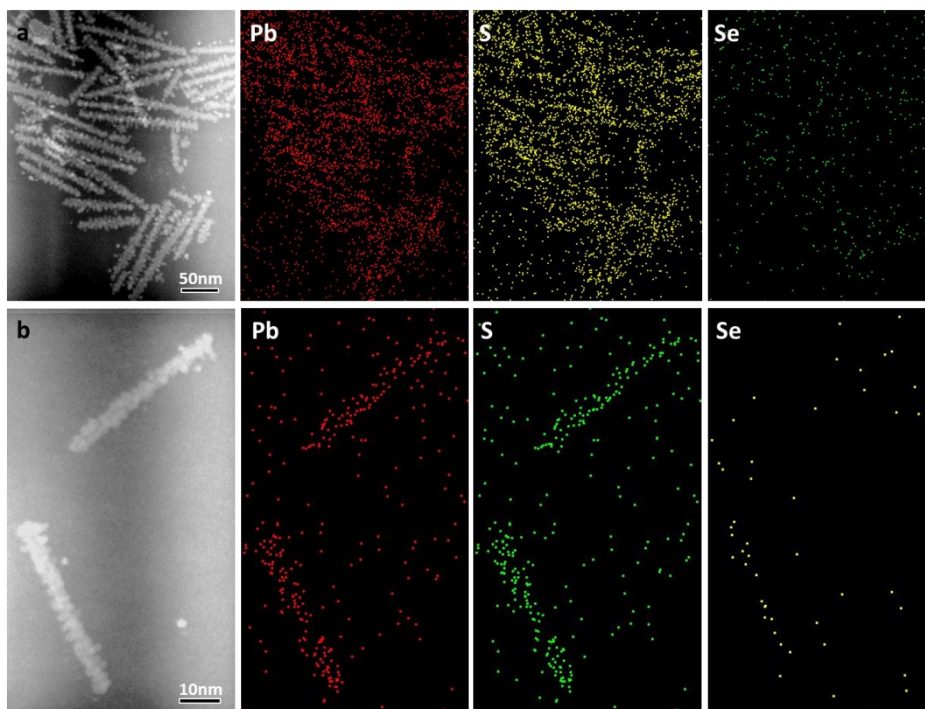


Figure S19. HAADF-STEM images and element maps of branched hetero- PbS-PbSe/PbS core/shell nanorod couples obtained after the cation exchange reaction. (a) Hetero- PbS-PbSe/PbS core/shell nanorod couples with a large population. (b) Two individual hetero- PbS-PbSe/PbS core/shell nanorod couples.

References

- 1 L. Carbone, C. Nobile, M. De Giorgi, F. Della Sala, G. Morello, P. Pompa, M. Hytch, E. Snoeck, A. Fiore, I. R. Franchini, M. Nadasan, A. F. Silvestre, L. Chiodo, S. Kudera, R. Cingolani, R. Krahne and L. Manna, *Nano Lett.*, 2007, **7**, 2942-2950.
- 2 G. Jia, A. Sitt, G. B. Hitin, I. Hadar, Y. Bekenstein, Y. Amit, I. Popov and U. Banin, *Nat. Mater.*, 2014, **13**, 301-307.
- 3 A. M. Smith, A. M. Mohs and S. Nie, *Nat. Nanotechnol.*, 2009, **4**, 56-63.
- 4 H. Zhong, T. Mirkovic and G. D. Scholes, *Comprehensive Nanoscience and Technology Vol. 5: Nanocrystal Synthesis*, (Eds: D. Andrews, G. Scholes, G. Wiederrecht), Elsevier 2010, 153-201.
- 5 C.-M. Ning, L. Dou and P. Yang, *Nat. Rev. Mater.*, 2017, **2**, 17070.
- 6 C. Tan, J. Chen, X.J. Wu and H. Zhang, *Nat. Rev. Mater.*, 2018, **3**, 17089.
- 7 G. Pellegrini, G. Mattei, P. and Mazzoldi, *J. Appl. Phys.*, 2005, **97**, 073706.
- 8 T. Omata, K. Nose and S. Otsuka-Yao-Matsuo, *J. Appl. Phys.*, 2009, **105**, 073106.
- 9 a) H. Landolt, R. Börnste and Landolt-Börnstein: Numerical Data and Functional Relationships in Science and Technology, O. Madelung, U. Rössler, M. Schulz, Ed. group III, vol. 41B (Springer, Berlin, 1982); b) Landolt-Börnstein: Numerical Data and Functional Relationships in Science and Technology, New Series (Ed: K. H. Hellwege), Springer, Berlin 1983.
- 10 M. Cardona, *J. Phys. Chem. Solid.*, 1963, **24**, 1543-1555.
- 11 S.H. Wei and A. Zunger, *Appl. Phys. Lett.*, 1998, **72**, 2011-2013.
- 12 H. E. Ruda, *J. Appl. Phys.*, 1986, **59**, 3516-3526.
- 13 Murayama, M. and Nakayama, T. *Phys. Rev. B* 1994, **49**, 4710-4724.